Removing the Gβγ-SNAP25 brake on exocytosis enhances insulin action, promotes adipocyte browning, and protects against diet-induced obesity

Ryan P. Ceddia[1,*], Zack Zurawski[2,3,*], Analisa Thompson Gray[2], Feyisayo Adegboye[2], Fubiao Shi[1], Dianxin Liu[1], Jose Maldonado[4], Julio E. Ayala[4], Owen P. McGuinness[4], Sheila Collins[1,4], Heidi E. Hamm[2]

[1]Department of Medicine, Division of Cardiovascular Medicine, Vanderbilt University Medical Center, Nashville, TN 37232, USA

[2]Department of Pharmacology, Vanderbilt University, Nashville, TN 37232, USA

[3]Department of Anatomy and Cell Biology, University of Illinois at Chicago, Chicago, IL 60612, USA.

[4]Department of Molecular Physiology and Biophysics, Vanderbilt University, Nashville, TN 37232, USA

*These authors contributed equally to this work.

Corresponding author and person to whom reprints should be addressed:

Heidi Hamm, Ph.D.

Vanderbilt University

442 Robinson Research Building Nashville, TN 37212

Tel: 615-343-9536

Email: heidi.hamm@vanderbilt.edu

Abstract

Negative regulation of exocytosis from secretory cells throughout the body is accomplished through inhibitory signals from $G_{i/o}$ G protein-coupled receptors by Gβγ subunit inhibition of two common mechanisms: (i) decreased calcium entry and (ii) direct interaction of Gβγ with the Soluble *N*-ethylmaleimide-sensitive factor Attachment Protein (SNAP) Receptor (SNARE) plasma membrane fusion machinery. We have previously shown that disabling the second mechanism with a truncation of SNAP25 ($SNAP25^{\Delta3/\Delta3}$) decreases the affinity of Gβγ for the SNARE complex, leaving exocytotic fusion as well as modulation of calcium entry intact. Here we report significant beneficial metabolic remodeling in mice carrying this mutation. Chow-fed $SNAP25^{\Delta3/\Delta3}$ mice exhibit enhanced insulin sensitivity and increased beiging of white fat. In response to a high fat diet, the metabolic protection was amplified in $SNAP25^{\Delta3/\Delta3}$ mice. Glucose homeostasis, whole body insulin action, and insulin-mediated glucose uptake into white adipose tissue were improved along with resistance to diet-induced obesity. This metabolic protection in $SNAP25^{\Delta3/\Delta3}$ mice occurred without compromising the physiological response to fasting or cold. All metabolic phenotypes were reversed at thermoneutrality, suggesting basal autonomic tone is required. Thus, the Gβγ-SNARE interaction represents a cellular mechanism that deserves further exploration as a new avenue for combatting metabolic disease.

GRAPHICAL ABSTRACT

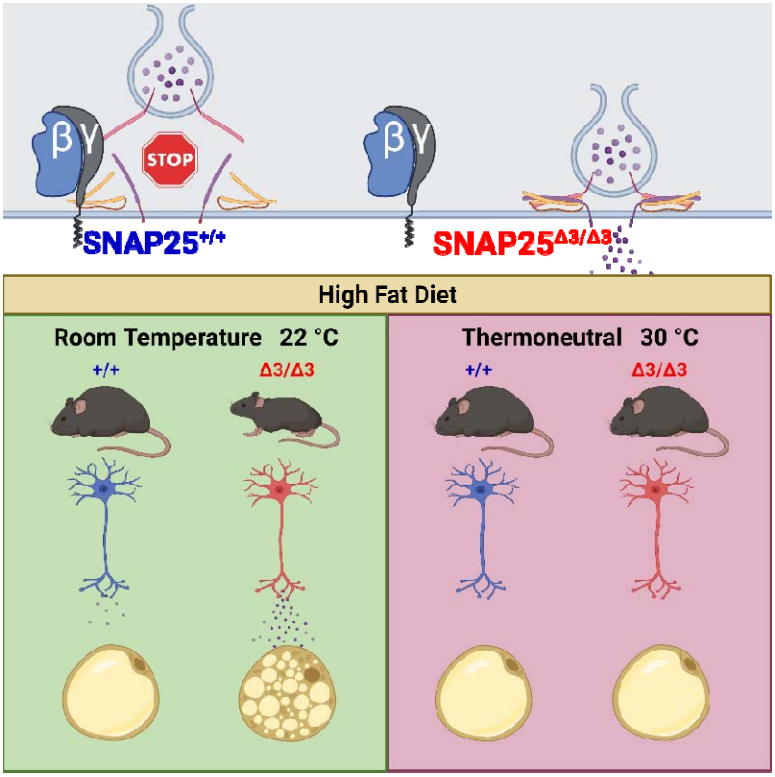

Introduction

Metabolic diseases, such as diabetes and obesity, have an estimated annual global economic impact in the trillions of (US) dollars (1-5). Therapeutic approaches to lower metabolic risk include augmenting insulin secretion, limiting adiposity either by suppressing food intake or augmenting energy expenditure, and/or by improving insulin action. G protein coupled receptors (GPCRs) in metabolically important target tissues such as the liver, brain, adipose tissue and pancreatic islets play critical roles in metabolic regulation and energy balance (6). Particularly in type 2 diabetes, pharmacologic agents have leveraged incretin-mediated GPCR signals to augment glucose-stimulated insulin secretion (GSIS) and attenuate weight gain (7). However, there may be additional approaches to manipulate GPCR signaling to treat metabolic disease.

GPCRs mediate downstream signaling events through the activation of heterotrimeric G proteins (e.g., Gα and Gβγ). Signaling events mediated by the classical Gα subunits are well known and targeting either the receptor or the Gα-generated signal in specific target tissues have been successful in many spheres of pharmacology including metabolic disease (8, 9). By contrast, signaling via the Gβγ-subunits has received less attention. They differ from Gα in their physiologic roles (10, 11). They transduce feedback signals that modulate or inhibit neurotransmitter and hormone secretion (12). One function of Gβγ is to inhibit exocytosis in endocrine and excitable cells. This Gβγ mechanism curbs GSIS in the pancreatic β-cell by either modulating calcium entry and/or by directly binding to the exocytotic fusion complex (13). In β-cells norepinephrine (NE) is thought to inhibit insulin exocytosis via the α_2-adrenergic receptor (AR) through the interaction of Gβγ and SNARE (13). We have shown in neurons that this inhibition requires Gβγ binding to the SNARE complex through the last three amino acids of SNAP25 (14, 15). To specifically study the contribution of Gβγ to the exocytotic fusion step *in vivo*, we developed an allele of SNAP25 encoding a protein that lacks these last three amino acids (therefore called the SNAP25Δ3 protein) and created a mouse where SNAP25Δ3 replaces SNAP25 on both alleles (16, 17). We have called this mouse $SNAP25^{\Delta3/\Delta3}$. We have previously shown that

SNAP25Δ3 can form SNARE complexes that undergo calcium-synaptotagmin mediated zippering and exocytosis identical to that of SNAP25, but its ability to interact with Gβγ, and the resulting GPCR-mediated inhibitory effect on exocytosis is disabled (14). Using the SNAP25$^{\Delta3/\Delta3}$ mouse we previously demonstrated the importance of the Gβγ-SNARE pathway in several signaling processes, including stress responses and pain processing, long-term potentiation and spatial memory (14, 18). However, the impact on metabolism and response to diet-induced obesity are unknown.

GPCR- and Gβγ-SNARE-dependent signals are involved in regulating metabolically important activities, such as feeding behavior, energy balance, insulin secretion and thermoregulation (19-24). The specific role Gβγ-SNARE-dependent signals play in regulating these physiologic responses are unknown. For example, when a palatable high fat diet (HFD) is made available, it is unknown if Gβγ-SNARE-dependent signals serve to limit or amplify weight gain or contribute to glucose dysregulation and metabolic inflexibility commonly seen in metabolic disease (25, 26). As Gβγ-SNARE-dependent signals can serve as physiological brakes, they may restrain insulin secretion, impair insulin action, limit satiety or attenuate energy expenditure, thus aggravating adiposity and impairing glucose homeostasis. We hypothesized that attenuation of this physiological brake using the SNAP25$^{\Delta3/\Delta3}$ mouse would improve glucose homeostasis and improve metabolic disease phenotypes in response to a palatable HFD. Our data demonstrate that chow-fed SNAP25$^{\Delta3/\Delta3}$ mice are more insulin sensitive and display increased adipose tissue beiging. Moreover, in response to a HFD challenge, the removal of this Gβγ-SNARE braking mechanism attenuates adiposity, improves insulin action, and amplifies sympathetic tone and subsequent browning of adipose tissue. Reducing autonomic tone by placing animals in a thermoneutral environment removes the metabolic protection afforded by this Gβγ-SNARE braking mechanism. The resistance to diet induced obesity (DIO) and improved glucose homeostasis when this braking mechanism is disabled suggest the Gβγ-SNARE interaction is a potential novel therapeutic target to treat metabolic disease.

Results

Normal growth curves with increased white adipose tissue beiging in chow-fed SNAP25$^{\Delta3/\Delta3}$ mice

Body weights of male and female SNAP25$^{\Delta3/\Delta3}$ mice were monitored over a 60-week period while being fed a standard chow diet; no differences were observed in growth curves compared to their SNAP25$^{+/+}$ littermates (**Fig. 1A; Fig. S1A**). Weights of internal organs and tissues were examined in a second cohort of 15-week-old mice. No statistically significant difference in most organ weights was observed in male mice. As there was a trend toward slightly smaller adipose depots in SNAP25$^{\Delta3/\Delta3}$ mice (**Fig. 1B**), we examined adipose histology. We observed a modest increase in UCP1-positive beige adipocytes in the inguinal white adipose tissue (iWAT) depot without an accompanying change in the interscapular brown adipose tissue (**Fig. 1C,D**). Consistent with a reduction in adipose tissue mass, we observed a decrease in the amount of circulating leptin (3.01 ± 0.46 vs. 1.24 ± 0.27 ng/ml leptin; *N* = 9 SNAP25$^{+/+}$ vs. 12 SNAP25$^{\Delta3/\Delta3}$ male mice; mean ± SEM; P = 0.002). These differences in adipose weight and remodeling were more evident in female mice (**Fig. S1**). A cohort of 15-week-old SNAP25$^{\Delta3/\Delta3}$ female mice weighed slightly less than SNAP25$^{+/+}$ mice (**Fig. S1B**) had smaller fat pads (**Fig. S1C**), and adipocyte size was reduced in both iBAT and iWAT (**Fig. S1D,E**). Though lacking a strong effect on the overall size and appearance of the mice, loss of the Gβγ-SNARE interaction leads to a reduction in the size of adipocytes and their fat pad depots, associated with increased WAT beiging.

Lower glucose stimulated insulin secretion in vivo, but not ex vivo, without defects in glucose regulation suggests improved insulin action in SNAP25$^{\Delta3/\Delta3}$ mice fed chow diet

To determine if disabling the Gβγ inhibition of SNARE-mediated exocytosis would improve glucose homeostasis in chow-fed mice, we measured circulating glucose and insulin during an intraperitoneal glucose tolerance test (IP-GTT; 2 mg/kg) in 14-week-old chow-fed (5 h fasted) mice. Glucose tolerance in the SNAP25$^{\Delta3/\Delta3}$ mice was not different from SNAP25$^{+/+}$ mice (**Fig. 2A**). While basal insulin levels in SNAP25$^{\Delta3/\Delta3}$ mice were unaltered, insulin concentrations were reduced during the

GTT compared to SNAP25$^{+/+}$ mice (**Fig. 2B**) consistent with an improved insulin action. Since the incretin effect is bypassed with IP injection of glucose, we performed an oral glucose tolerance test in a separate cohort of chow-fed mice to test whether this approach might unmask an augmentation of insulin secretion in the SNAP25$^{\Delta3/\Delta3}$ mice (27). Oral glucose tolerance was again not different between genotypes (**Fig. 2C**). However, as was observed with the IP route of delivery, plasma insulin levels were lower in SNAP25$^{\Delta3/\Delta3}$ mice after the glucose gavage (**Fig. 2D**). The lower levels of insulin with a normal glucose tolerance are consistent with improved insulin sensitivity in SNAP25$^{\Delta3/\Delta3}$ mice.

There was no augmentation of insulin secretion during the GTT *in vivo (Fig. 2B,2D),* although this could be explained by an accompanying improvement in insulin action. Other investigators reported in a cell line that inhibition of insulin exocytosis by NE via α_2AR signaling was mediated by the Gβγ-SNARE interaction (13). We sought to determine in isolated perifused islets if loss of the Gβγ-SNARE interaction altered GSIS and α_2AR dependent inhibition of GSIS. We used a selective α_2AR agonist brimonidine (Br) to test this interaction. As shown in **Fig. 3A** and **3B**, GSIS in isolated islets from SNAP25$^{\Delta3/\Delta3}$ mice was not greater than from SNAP25$^{+/+}$ mice. Moreover, contrary to earlier studies in an immortalized mouse β-cell line (13), Br was able to equally suppress GSIS in islets from SNAP25$^{\Delta3/\Delta3}$ and SNAP25$^{+/+}$ mice (**Fig. 3A,C**). Insulin content of the islets was also not significantly affected by SNAP25 genotype (**Fig. 3D**). This indicates that α_2AR-mediated signaling in *ex vivo* mouse islets is able to inhibit GSIS via a mechanism that is independent of the Gβγ-SNARE interaction.

Unaltered energy expenditure at room temperature and in response to cold in SNAP25$^{\Delta3/\Delta3}$ mice fed chow diet

We assessed if disabling of this Gβγ-SNARE interaction altered the response to physiologic stressors, since we had previously reported that SNAP25$^{\Delta3/\Delta3}$ mice had an altered behavioral response to acute physiological stressors, specifically elevated stress-induced hyperthermia (14, 18). We performed calorimetry studies in which energy expenditure and feeding behavior in chow-fed SNAP25$^{+/+}$ and SNAP25$^{\Delta3/\Delta3}$ mice were measured at standard housing temperature (22°C). The mice

were then exposed to an acute cold challenge (6°C) to assess whether they could mount a physiologic response by increasing energy expenditure and food intake. At normal housing temperature SNAP25$^{\Delta3/\Delta3}$ mice had similar rates of energy expenditure (**Fig. S2A**) and food intake (**Fig. S2B**), with normal diurnal patterns for both variables. In response to a decrease in environmental temperature both SNAP25$^{\Delta3/\Delta3}$ mice and their SNAP25$^{+/+}$ littermates mounted a robust increase in energy expenditure. This was also accompanied by a greater increase in the duration of feeding activity in SNAP25$^{\Delta3/\Delta3}$ mice (**Fig. S2E**). Interestingly, any changes in autonomic tone that might occur are not global. For example, in a separate cohort, cardiovascular parameters were measured at standard housing temperature using echocardiography, and no differences were observed in the SNAP25$^{\Delta3/\Delta3}$ mice (**Fig. S3**). Thus, on a chow diet SNAP25$^{\Delta3/\Delta3}$ mice display subtle changes in feeding behavior that overall do not impact energy balance; the physiologic autonomic dependent response to cold is also intact.

Protection from high fat diet-induced obesity and adiposity in SNAP25$^{\Delta3/\Delta3}$ mice

Given the apparent greater insulin sensitivity of the SNAP25$^{\Delta3/\Delta3}$ mice when on chow diet (**Fig. 2**) we tested whether this phenotype would persist when challenged with a HFD. We focused on male mice given the robust improvement in insulin action observed on a chow diet. Eight-week-old SNAP25$^{+/+}$ and SNAP25$^{\Delta3/\Delta3}$ mice were provided a HFD for 8 weeks. As shown in **Fig 4A**, SNAP25$^{+/+}$ mice rapidly gained weight on the HFD, whereas SNAP25$^{\Delta3/\Delta3}$ mice were markedly resistant to HFD-induced weight gain. Body composition analyses revealed that the reduced weight gain in SNAP25$^{\Delta3/\Delta3}$ mice was due to reduced adiposity (**Fig. 4B**). This was reflected in a decrease in plasma leptin (14.3 ± 1.32 vs. 3.53 ± 1.23 ng/ml leptin; N = 9 SNAP25$^{+/+}$ vs. 7 SNAP25$^{\Delta3/\Delta3}$; mean ± SEM; $P < 0.001$). This was confirmed in postmortem analyses of these mice. In addition to a reduction in the weight of all fat depots (epididymal WAT; eWAT, inguinal WAT; iWAT, retroperitoneal WAT; rpWAT, and interscapular BAT; iBAT), liver weight and hepatic steatosis were also reduced in SNAP25$^{\Delta3/\Delta3}$ compared to SNAP25$^{+/+}$mice (**Fig. 4C,D**). The size of the kidney, spleen, heart, and most skeletal muscles were unaffected (**Fig. 4D**).

Improvement in insulin action in SNAP25$^{\Delta3/\Delta3}$ mice following high fat diet challenge

Having observed a profound difference in weight gain and adiposity in SNAP25$^{\Delta3/\Delta3}$ mice when challenged with a HFD, we hypothesized that glucose homeostasis would also be improved. Indeed, HFD-fed SNAP25$^{\Delta3/\Delta3}$ mice showed a significant improvement in the IP-GTT (**Fig. 5A**) compared with SNAP25$^{+/+}$ mice. SNAP25$^{\Delta3/\Delta3}$ mice had lower 5 h fasting glucose levels (**Fig. 5B**), congruent with their lower IP-GTT curves. Plasma insulin was also significantly lower (**Fig. 5B**). Together, these data indicate that there is a *bona fide* improvement in insulin sensitivity of the SNAP25$^{\Delta3/\Delta3}$ mice.

To determine the contribution of specific tissues to the improved glucose homeostasis of SNAP25$^{\Delta3/\Delta3}$ mice, we performed hyperinsulinemic euglycemic clamps in chronically catheterized conscious mice that had been consuming the HFD for 8 weeks (40.9 ± 2.5 vs. 27.2 ± 0.8 g body weight; SNAP25$^{+/+}$ vs. SNAP25$^{\Delta3/\Delta3}$; mean ± SEM). We determined if insulin suppression of endogenous (i.e. hepatic) glucose production and/or stimulation of peripheral glucose uptake were altered. Arterial insulin levels were lower in the basal period in SNAP25$^{\Delta3/\Delta3}$ (5.8 ± 1.1 vs. 2.5 ± 0.2 ng/ml; SNAP25$^{+/+}$ vs. SNAP25$^{\Delta3/\Delta3}$; mean ± SEM) and increased with insulin infusion during the clamp period (9.7 ± 1.7 vs. 5.1 ± 0.8 ng/ml; SNAP25$^{+/+}$ vs. SNAP25$^{\Delta3/\Delta3}$; mean ± SEM). Arterial blood glucose was maintained at euglycemia in both groups throughout the clamp procedure (**Fig. 5C**). The glucose infusion rate required to maintain euglycemia was increased in SNAP25$^{\Delta3/\Delta3}$ despite lower clamp insulin concentrations (**Fig. 5C**). Using [3-^{3}H]-glucose to assess whole body glucose flux we determined that the increase in glucose requirements in SNAP25$^{\Delta3/\Delta3}$ resulted from an increase in whole body glucose uptake (**Fig. 5D**). Basal endogenous glucose production as well as insulin suppression of endogenous glucose production were comparable (**Fig. 5D**). Note, however, there was a shift to the left in the relationship between insulin and glucose production as well as uptake. This indicates both hepatic and peripheral tissues of SNAP25$^{\Delta3/\Delta3}$ mice were more sensitive to insulin. To determine which tissues contributed to the increase in glucose disposal we assessed glucose uptake (Rg) in multiple tissues during the clamp using [^{14}C]2-deoxy-D-glucose (2-DG). Rg was markedly increased in SNAP25$^{\Delta3/\Delta3}$

mice in multiple skeletal muscles (soleus, and vastus lateralis) and white adipose tissue depots (perigonadal eWAT and subcutaneous iWAT) (**Fig. 5E**). Rg was unchanged in the interscapular brown adipose tissue (iBAT), heart, gastrocnemius and brain. Together, these data suggest that despite much lower insulin levels during the clamp period, multiple tissues of SNAP25$^{\Delta3/\Delta3}$ mice are more responsive to insulin than SNAP25$^{+/+}$ mice.

Elevation of autonomic tone and increased beiging of white adipose tissue in SNAP25$^{\Delta3/\Delta3}$ mice following high fat diet challenge

We then sought to investigate the changes that may have occurred in the adipose tissue of the SNAP25$^{\Delta3/\Delta3}$ mice that could enhance their response to insulin and augment glucose uptake. As has been observed in humans, increased beiging and the accompanying remodeling of the white adipose depots to be more oxidative may be responsible for some of the increased glucose uptake into WAT in SNAP25$^{\Delta3/\Delta3}$ mice (28). Indeed, as in the chow-fed mice, HFD-fed SNAP25$^{\Delta3/\Delta3}$ mice exhibited increased iWAT beiging (**Fig. 6B**). Adipocyte size was significantly reduced in both iWAT and iBAT as indicated by an increase in the density of nuclei (hematoxylin) relative to the area of tissue (**Fig. 6C,D**). The iBAT of HFD-fed SNAP25$^{+/+}$ mice had many large unilocular adipocytes, whereas SNAP25$^{\Delta3/\Delta3}$ had smaller multilocular adipocytes (**Fig. 6A**). Recent studies have observed an increase in the quantity of sympathetic nerve endings in beiged adipose tissue (29-34). Consistent with this, immunohistochemical staining of adipose tissue sections for Tyrosine Hydroxylase (TH), the first and rate-limiting enzyme in the catecholamine biosynthesis pathway, showed a significant increase in the number of sympathetic boutons identified by TH staining in both iBAT and iWAT (quantified in **Fig. 6C,D**). This increase in TH-positive en-passant nerve endings and boutons in the iWAT is evident both in the stained sections (**Fig. 6B,D**).

The adipo-clear method and three-dimensional imaging were used to visualize the complete sympathetic innervation and beiging of iWAT from SNAP25$^{+/+}$ and SNAP25$^{\Delta3/\Delta3}$ mice (**Fig. 7**). As we had seen previously, iWAT from chow-fed SNAP25$^{+/+}$ and SNAP25$^{\Delta3/\Delta3}$ mice were superficially very

similar (**Fig. 7A-B,E-F, Movie 1,2**). Upon HFD challenge, SNAP25$^{+/+}$ iWAT exhibited a reduction in sympathetic innervation (**Fig. 7C,G, Movie 3**), which has been well established (35, 36). The iWAT from SNAP25$^{\Delta3/\Delta3}$ mice exhibited some remodeling due to HFD, but this was much reduced compared to SNAP25$^{+/+}$ and sympathetic neurons remained abundant and strongly stained for TH (**Fig. 7D,H, Movie 4**). Adipocyte beiging, and consequently UCP1 staining, is heterogeneous by nature exhibiting a 'patchy' appearance which we observe in iWAT from all four conditions. By imaging entire iWAT depots we are able to eliminate sampling bias due to the patchy distribution of UCP1-positive adipocytes, observeing UCP1 staining congruent with our standard two-dimensional histology. Notably, iWAT from HFD-fed SNAP25$^{\Delta3/\Delta3}$ mice, as opposed to their SNAP25$^{+/+}$ counterparts, continue to exhibit extensive UCP1 staining confirming that the SNAP25Δ3 mutation facilitates beiging throughout the entire iWAT depot (**Fig. 7D,H**).

Many hormones that elicit adipose tissue browning do so through the cyclic nucleotide-PKA (or PKG) signaling pathway (6, 37). To visualize the amount of PKA signaling in these tissues, we performed a Western Blot for the phosphorylated PKA target sequence in iBAT, iWAT, and eWAT (**Fig. 6E**). HFD appeared to reduce phosphorylation of the PKA target sequence, perhaps due to previously shown reductions in levels of βAR subtypes in adipose tissues of obese mice (38-40). This decrease in PKA phosphorylation tended to be restored by the SNAP25$^{\Delta3/\Delta3}$ mutation and some depots in SNAP25$^{\Delta3/\Delta3}$ mice even appeared to have increased phosphorylation in the chow-fed state. As the catecholamine NE is released from synaptic vesicles in sympathetic neuronal endings and classically induces PKA signaling in adipose tissue, we measured catecholamines by high-performance liquid chromatography (HPLC) in these HFD-fed mice. Though circulating catecholamines were unchanged (**Fig. S4**), measurements directly from homogenized iWAT (2.06 ± 0.26 vs. 47.20 ± 9.61 ng/mg; SNAP25$^{+/+}$ vs. SNAP25$^{\Delta3/\Delta3}$; mean ± SEM) revealed a 23-fold increase in NE **(Fig. 6F).** Collectively, these data indicate that SNAP25$^{\Delta3/\Delta3}$ mice have an elevated autonomic tone and this excess NE in the adipose tissues promotes PKA signaling and beiging.

Attenuation of the acute hyperphagic response to high fat diet in SNAP25$^{\Delta3/\Delta3}$ mice

To determine the mechanism for the relative reduction in weight gain and fat mass in SNAP25$^{\Delta3/\Delta3}$ mice, we assessed lipid absorption, food intake, and energy expenditure in mice on HFD. Fecal triglyceride content was not different (1.10 ± 0.29 vs. 0.86 ± 0.21 µg triglyceride/mg feces; *N* = 8 SNAP25$^{+/+}$ vs. 7 SNAP25$^{\Delta3/\Delta3}$; mean ± SEM; P = 0.526), indicating that the reduction in body weight in SNAP25$^{\Delta3/\Delta3}$ mice was not due to a decrease in lipid absorption by the gut . We examined food intake over the first 5 weeks as chow-fed mice were switched to a HFD (**Fig. 8A**). During the first two weeks of HFD, SNAP25$^{+/+}$ mice exhibit a robust increase in food intake, this is commonly observed in wild-type mice presented with a palatable HF diet. However, this was attenuated in SNAP25$^{\Delta3/\Delta3}$ mice (**Fig. 8A**). By the third week, the hyperphagia in the SNAP25$^{+/+}$ mice had diminished, and by week 4 the two genotypes consumed similar amounts of HFD. Energy expenditure and food intake follow a diurnal pattern with both being highest during the dark phase. We repeated the study while housing the mice in the Promethion calorimetry system where we could continuously monitor diurnal feeding patterns and energy expenditure as animals were transitioned from chow to HFD. This allowed us to determine if the genotype affected the diurnal patterns (**Fig. 9**). Chow-fed mice were monitored for 5 days and then switched to a HFD for 12 days. Energy expenditure was not different and was highest in the dark phase in both genotypes on a chow diet (**Fig. 9B**). When presented with a HFD both genotypes showed a robust and comparable increase in energy expenditure and caloric intake (**Fig. 9B,C**). This was evident during the light phase but not the dark phase. While energy expenditure did not differ between genotypes during the 12 days on a HFD (**Fig. 9B**), the initial hyperphagia gradually subsided in the SNAP25$^{\Delta3/\Delta3}$ to a greater extent than in SNAP25$^{+/+}$ mice (**Fig. 9C**). The 12-day cumulative caloric intake (**Fig. 9A**), and consequently adiposity (**Fig. 9E**), was decreased in SNAP25$^{\Delta3/\Delta3}$ mice. Thus, SNAP25$^{\Delta3/\Delta3}$ mice have a short-term but significantly altered food consumption pattern, which contributes to the reduced weight gain on a HFD. To assess more empirically whether the SNAP25$^{+/+}$ mice are unable to mount a robust hyperphagic response we utilized a fasting-refeeding paradigm

where animals were fasted for 12 h and then presented with a HFD (**Fig. 8B**). Both genotypes had an equivalent and marked increase in HFD consumption over a 4-hour period. To assess food preference, we presented SNAP25$^{\Delta3/\Delta3}$ mice and their SNAP25$^{+/+}$ littermates with HFD and chow in tandem and monitored total intake of both diets and body weight **(Fig. 8C**). No significant differences were identified based on genotype. Taken together, we can infer that altered feeding behavior in response to a HFD in SNAP25$^{\Delta3/\Delta3}$ mice is a contributor to the differential weight gain phenotype. However, this initial response is not driven by an aversion to a HFD or the inability to mount a hyperphagic response.

Reversal of metabolic protection in male SNAP25$^{\Delta3/\Delta3}$ mice by thermoneutral housing conditions

A mild thermogenic stress is evoked in mice by housing at standard room temperature (~22 °C); this requires activation of the autonomic nervous system in adipose and other tissues to support thermoregulation (41). Increased autonomic tone and beiging of adipose tissue are observed in the SNAP25$^{\Delta3/\Delta3}$ mice housed at standard housing conditions (**Fig. 6**), suggesting that the Gβγ-SNARE interaction is a negative regulator of autonomic tone. We hypothesized that if we minimized the induction of autonomic drive by shifting animals to a thermoneutral setting (~30 °C) the metabolic benefits of SNAP25$^{\Delta3/\Delta3}$ would decrease. Therefore, we housed SNAP25$^{\Delta3/\Delta3}$ mice and their SNAP25$^{+/+}$ littermates in thermoneutral housing and exposed them to a HFD. Indeed, the weight gain, adiposity and increased fat pad and liver size in response to a HFD of SNAP25$^{\Delta3/\Delta3}$ mice (**Fig. 10A-C**) were eliminated. Food intake in response to HFD feeding was also not different between genotypes during the thermoneutral housing conditions (**Fig. 10D**). Thermoneutral housing did not revert SNAP25$^{\Delta3/\Delta3}$ food intake to SNAP25$^{+/+}$ room temperature levels; instead in both genotypes food intake was lower than in room temperature housed animals during all weeks of the study (**Fig. 8A, 10D**). Improvements in insulin action during IP-GTT, in both the chow and HFD feeding period, were abolished by housing the mice in thermoneutral conditions (**Fig. 10E,F**). These findings demonstrate that the metabolic improvements caused by removing the Gβγ-SNARE interaction are dependent upon the environmental temperature in which the mice are housed. This is consistent with our hypothesis that increased

sympathetic tone due to loss of the α_{2A}-adrenergic brake to exocytosis mediates the metabolic protection conferred in SNAP25$^{\Delta3/\Delta3}$ mice.

Prevention of diet induced remodeling of adipose tissues in SNAP25$^{\Delta3/\Delta3}$ mice by thermoneutral housing conditions

Increasing sympathetic tone to induce heat production from adipose tissue is a fundamental part of the response to environmental cold stress (42, 43). The dysregulation of autonomic tone in SNAP25$^{\Delta3/\Delta3}$ mice is most apparent in the adipose tissue of HFD-fed mice housed at room temperature as these have increased beiging and high adipose tissue NE (**Fig. 6**). In the mice housed at thermoneutral conditions, this adipose beiging and elevation of NE content is eliminated (**Fig. 11A-E**). Both iBAT and iWAT from SNAP25$^{\Delta3/\Delta3}$ mice are appropriately remodeled in response to HFD feeding (**Fig. 11A-D**), but no difference is seen between the genotypes. The adipocyte sizes may be slightly smaller in SNAP25$^{\Delta3/\Delta3}$ depots, but this difference is not significant as determined by the density of the nuclei (iBAT: 611 ± 95 vs. 798 ± 67 hematoxylin/mm^2, iWAT: 114 ± 7.4 vs. 127 ± 19 hematoxylin/mm^2; mean ± SEM; iBAT P = 0.1590, iWAT P = 0.5755) (**Fig. 11C,D**). Housing at thermoneutrality eliminated the increase in adipose tissue NE levels (**Fig. 11E**). The ability of thermoneutral housing conditions to reverse the metabolic improvements achieved by disrupting the Gβγ-SNARE interaction indicates that these improvements are caused by an elevation of autonomic tone in adipose tissue We posit that loss of the brake to SNARE-mediated vesicle fusion and neurotransmitter release by Gβγ in SNAP25$^{\Delta3/\Delta3}$ mice causes prolonged release, and therefore larger overall amounts, of neurotransmitters (**Fig. 11F**). NE induction of adipose tissue beiging and the thermogenic program in SNAP25$^{\Delta3/\Delta3}$ mice likely contribute to improvements in insulin action particularly in the adipose tissue. This increased sympathetic neural drive causes SNAP25$^{\Delta3/\Delta3}$ mice, which only that lack the inhibitory actions of Gβγ on the SNARE complex, to be remarkably resistant to diet induced obesity and the associated impairment in glycemic control.

Discussion

Hormones that activate GPCRs have long been known to be important positive modulators of signals in cell types that can impact metabolic disease risk (44). We demonstrate that targeting negative feedback circuits that signal through the Gβγ-SNARE complex amplifies autonomic tone by removing the braking effect of the α_{2A} adrenergic autoreceptor, which we have shown works through the Gβγ-SNARE interaction mechanism (14), leading to physiological benefits on metabolism. By utilizing a mouse model that is deficient in the Gβγ-SNARE interaction, we investigated the specific role of Gβγ inhibition of SNARE-mediated vesicle release on glucose handling, adiposity and energy balance (14). In lean chow-fed mice, disabling this braking mechanism induced beiging of adipose tissue depots with an accompanying improvement in insulin action. In response to a HFD the metabolic protection persisted and in fact was amplified by an attenuation of body weight gain. This metabolic protection leverages basal autonomic tone; removal of autonomic tone by placing mice in a thermoneutral environment removes the metabolic protection that is afforded by disabling this braking mechanism. These data suggest a unique physiological role for Gβγ modulation of exocytosis via the SNARE complex might be leveraged to improve metabolic disease.

Our data show that adipose tissue beiging is a characteristic feature of removal of the Gβγ-inhibition of SNARE-mediated exocytosis of NE. In both chow-fed and HFD-fed mice, adipose tissue NE content was increased with corresponding increased TH staining indicative of increased sympathetic outflow to adipose tissue. Adipose tissue was extensively remodeled. The adipocytes were smaller and exhibited a beiging and more oxidative phenotype (increased UCP1) (19). In BAT the change is less profound primarily impacting UCP1; this may be because at standard housing conditions BAT is already partially differentiated (45). This beiging phenotype of WAT was amplified in the setting of a HFD. An increase in sympathetic nerve activity in white adipose is likely the major driver of adipose tissue remodeling (19, 39). This likely reflects an attenuation of the inhibitory effects of NE via α_2-adrenergic signaling on exocytosis of neurotransmitters. Consistent with an adrenergic driven process

this response was attenuated by housing mice in a thermoneutral environment. Thus, the extensive remodeling of WAT requires basal autonomic activity with which to amplify the adipose tissue remodeling with removal of the Gβγ-inhibition of SNAP25 interaction.

Insulin action was markedly improved with removal of the Gβγ-inhibition of SNARE-mediated exocytosis. Fasting glucose and insulin were unaffected in chow-fed animals. The insulin response required to dispose of a glucose load, while maintaining normal glucose tolerance, was decreased in SNAP25$^{\Delta3/\Delta3}$ mice. This indicates that insulin dependent glucose disposal was augmented. The lack of a change in basal insulin or glucose in chow-fed mice suggests the benefit is primarily in peripheral tissues and not in the liver. The deletion of the Gβγ-SNARE interaction plays its most important role in amplifying the metabolic flexibility of the organism to handle a carbohydrate load. In response to a HFD, this protection is enhanced, with global improvement in insulin action in multiple tissues including liver, muscle and WAT. The potency of the metabolic protection obtained as WAT remodels to a more oxidative phenotype is remarkable given the relatively low-fat mass in chow-fed mice. However, this is consistent with multiple reports. When investigators directly targeted adipose tissue to augment beiging, insulin action improved even in lean mice (28). The real benefit of beiging in this context appears to be creating a metabolic sink for insulin stimulated glucose disposal (46, 47). This benefit on insulin action is further amplified in HFD-fed mice by the attenuated weight gain in SNAP25$^{\Delta3/\Delta3}$ mice.

Physiologic beiging of adipose tissue depots did not lead to a measurable increase in whole body energy expenditure in SNAP25$^{\Delta3/\Delta3}$ mice. Using the Promethion indirect calorimetry system we assessed energy expenditure over multiple days in chow-fed mice, in response to a cold challenge as well as during the transition to a HFD. We used lean body mass as the covariate when we statistically analyzed the data using ANCOVA, as this is best practice when animals differ in either body weight or composition (48, 49). The lack of an increase in energy expenditure in SNAP25$^{\Delta3/\Delta3}$ mice relative to SNAP25$^{+/+}$ mice may be explained by the fact that the mass of adipose tissue that was affected in the lean and obese animal is quite small relative to the more oxidative skeletal muscle. More importantly, the increase in net autonomic tone was modest as it did not increase BAT glucose uptake during a

clamp in standard housing temperature despite further augmentation of UCP1 expression. This contrasts with the response to a cold environment, which robustly increases energy expenditure in part via activation of metabolism in BAT depots. The increase in energy expenditure in response to cold exposure also was not amplified in SNAP25$^{\Delta3/\Delta3}$ mice.

In our prior work we observed that SNAP25$^{\Delta3/\Delta3}$ mice have behavioral phenotypes that impact learning, memory, and responses to stressors (14, 18). One might anticipate that given the role of exocytosis in many physiologic systems, SNAP25$^{\Delta3/\Delta3}$ mice might have abnormal growth or feeding patterns or an inappropriate autonomic response to thermal stress. In fact, chow-fed male and female SNAP25$^{\Delta3/\Delta3}$ mice have normal growth curves and display normal circadian patterns of feeding and energy expenditure. When presented with a HFD, both SNAP25$^{\Delta3/\Delta3}$ and SNAP25$^{+/+}$ littermates have an initial robust increase in intake during the first 24h. However, intake gradually abates more rapidly in SNAP25$^{\Delta3/\Delta3}$ mice than in SNAP25$^{+/+}$ littermates. This leads to a decrease in cumulative intake and attenuation of diet-induced obesity. In response to cold stress, they can mount an appropriate increase in both food intake and energy expenditure. After an extended fast they exhibit a normal robust increase in food intake similar to SNAP25$^{+/+}$ littermates implying there is no amplification of gastrointestinal reflexes. When presented with a choice of a HFD or a chow diet they exhibited a normal intake of both the chow and HFD indicating they did not have an aversive response to the novel HFD. While autonomic tone was increased in adipose, this did not spillover to increase plasma catecholamines or result in abnormal cardiac function. Thus, overall SNAP25$^{\Delta3/\Delta3}$ mice retain physiologically normal metabolic and cardiovascular function.

We expected that the SNAP25$^{\Delta3/\Delta3}$ mice would exhibit improved GSIS because Gβγ has been reported to be a regulator of insulin exocytosis (13). Instead, we found that there was no augmentation of GSISin isolated islets from SNAP25$^{\Delta3/\Delta3}$ mice. Furthermore, α_2AR-mediated inhibition of GSIS was unaltered. One possible explanation for our results in islets is that the prior work on Gβγ was done in immortalized β-cell culture systems, which may not represent the interactions seen in islets. Another possibility is that in β-cells another protein (e.g. syntaxin 4, Munc18c) provides the scaffolding for the

Gβγ interaction with insulin granules (50-52). For example, in β-cells a second SNARE isoform such as SNAP23 could provide the scaffolding for the Gβγ interaction with insulin granules (53). While syntaxin1-SNAP25 is robustly regulated by Gβγ, islet t-SNARE pairs such as syntaxin4-SNAP25 may not be regulated in the same way(50). In addition to these *ex-vivo studies*, we examined GSIS *in-vivo*. Contrary to our expectations, *in vivo* GSIS was reduced even when we used an oral glucose tolerance test, which would amplify GPCR mediated signals to the endocrine pancreas. This led us to conclude that β-cell function is normal and SNAP25$^{\Delta3/\Delta3}$ mice have improved insulin-dependent glucose uptake. It is possible the underlying improvement in insulin action masked the physiological impact of the Gβγ-SNARE interaction to augment insulin secretion. Specific targeting of the SNAP25 in β-cells could determine if this interaction has a modulatory effect on insulin secretion *in vivo*.

SNAP25$^{\Delta3/\Delta3}$ mice were remarkably resistant to weight gain when challenged with a HFD, a phenotype that was reversed by thermoneutrality. We first asked if this phenotype was driven by alterations in energy intake as there was no alteration in gut absorption of dietary triglycerides. The initial hyperphagia seen in SNAP25$^{+/+}$ mice in response to a HFD was similar in SNAP25$^{\Delta3/\Delta3}$ mice. However, after 1 week the hyperphagia was less robust in the SNAP25$^{\Delta3/\Delta3}$ mice. As we already discussed, whole body energy expenditure was not increased. We calculated net energy balance (total energy expenditure-caloric intake). SNAP25$^{+/+}$ after 12 days on HFD tended to remain in a more positive energy balance than SNAP25$^{\Delta3/\Delta3}$ mice (6.2±1.9 vs 2.7±0.7 kcal/day; p=0.08; SNAP25$^{+/+}$ vs. SNAP25$^{\Delta3/\Delta3}$). This initial relative hypophagia in SNAP25$^{\Delta3/\Delta3}$ mice likely contributes to their resistance to HFD-induced obesity; the fact that it is reversed at thermoneutrality suggests it is controlled by sympathetic tone. It is possible that subtle and undetected increases in energy expenditure secondary to beiging will synergize with the attenuated intake to further limit weight gain. In response to weight gain endocrine signals such as leptin can serve as a brake to weight gain by limiting food intake and sustaining energy expenditure (54). An inappropriate increase in leptin in SNAP25$^{\Delta3/\Delta3}$ mice could limit adiposity. However, leptin was appropriately decreased paralleling the decrease in adiposity in SNAP25$^{\Delta3/\Delta3}$ mice. Given the impact of central autonomic drive in modulating food intake and energy

expenditure, future studies could target specific brain regions to determine the site of the amplification that restrains food intake.

These findings highlight the importance of the Gβγ-SNARE interaction in the regulation of insulin action and energy balance. A driver of this metabolic protection is increased autonomic tone and accompanying beiging of adipose tissue, which improves insulin action and glucose disposal. In the setting of a HFD challenge, the protection from weight gain in SNAP25$^{\Delta 3/\Delta 3}$ synergizes with the adipose beiging phenotype to further strengthen insulin action and improve glycemic control. Interestingly, this protection occurred by modulating a GPCR mediated signal rather than driving any specific receptor signaling pathway (55, 56). Importantly, this may explain why there were no apparent deleterious cardiac effects in these mice. Our findings parallel those of a recent study which used a brain-sparing sympathofacilitator to increase autonomic tone in mice with both studies observing increases in WAT NE levels and resistance to diet induced obesity without adverse cardiac effects (57). Recent work in humans has used β_3AR selective agonists in an effort to positively impact metabolic disease (58, 59). Similar to what we observed with targeting the Gβγ-SNARE interaction, an improvement in insulin action is the principal driver of the metabolic benefit (58). While there are many pathways that may be targeted to remodel adipose tissue metabolism, these same signaling pathways are also heavily involved in various physiological processes in other tissues; this constrains their clinical utility without tissue specificity (6, 44). Pharmacological targeting of the Gβγ-SNARE interaction is an interesting alternative to directly targeting the GPCRs themselves. This is because SNAP25$^{\Delta 3/\Delta 3}$ mice have broad improvements in food intake, activity, and adipose browning. Any potential neurological side effects could be ameliorated through designing CNS sparing agents. Thus, the approach of targeting a pathway that modulates rather than drives specific neuroendocrine signals is a novel approach to treat metabolic disease.

Materials and Methods

Animal procedures

All animal studies were conducted at Vanderbilt University. Mice used for these experiments were generated from heterozygous breeding of SNAP25$^{+/\Delta 3}$ mice on a C57BL/6 background. The strategy for the generation of these mice was previously described (14). Mice were maintained on a 12-hour light, 12-hour dark cycle and housed with 3–5 animals per cage except during monitoring of feed intake when they were singly housed. Mice were housed at standard housing room temperature (~22 °C) or thermoneutral housing conditions (~29.5 °C) when indicated. Mice were maintained *ad libitum* on chow (13.5% calories from fat: 5001; LabDiet) or high fat diet (HFD) (60% calories from fat: 3282; Bio-Serv) when indicated. Mice were weighed when indicated and body composition was measured using a LF50 Body Composition Analyzer (Bruker) at Vanderbilt Mouse Metabolic Phenotyping Center. All studies were performed with littermates of the appropriate genotypes. Mice were fasted 5h and euthanized by isoflurane overdose or CO_2 asphyxiation and exsanguination via cardiac puncture at the end of the study for collection of blood and tissues. Data from one mouse was excluded from all studies due to hydronephrosis. All procedures were approved by the Institutional Animal Care and Use Committee at Vanderbilt University.

Histology

Adipose tissues were fixed in 10% formaldehyde overnight and subsequently stored in 70% ethanol then processed routinely, embedded, sectioned and stained with hematoxylin and eosin (H&E) or immunohistochemically stained for Tyrosine Hydroxylase (ab152, Millipore Sigma) or UCP1 (ab10983, Abcam). Histology was performed by the Vanderbilt Translational Pathology Shared Resource. Whole slides were imaged at 20× with a Leica SCN400 Slide Scanner by the Digital Histology Shared Resource at Vanderbilt University Medical Center.

Quantification of TH staining was performed in QuPath version 0.3.0. One whole section of iWAT and iBAT were quantified for each mouse. Blood vessels, lymph nodes, and dissection artifacts were manually excluded from analysis. For all slides, hematoxylin stain was set at 0.63 0.682 0.371 and TH

stain was set at 0.479 0.618 0.623. Counting was performed using the Fast Cell Counts (Brightfield) feature. Cell detection threshold was set at 0.3 and DAB threshold was set at 0.6. All other parameters were the default values.

Leptin

At the end of the chow or HFD feeding studies, mice were euthanized as described and blood was obtained postmortem by terminal cardiac puncture and placed into a microcentrifuge tube coated with EDTA. Samples were kept on ice until centrifugation to obtain plasma which was stored at -80 °C. Leptin was measured from this plasma with a Luminex 100 system (Luminex Corp) at the Vanderbilt University Hormone Assay and Analytical Services Core.

Glucose tolerance test

For all glucose tolerance tests (GTT), mice were fasted for 5 h, and fasting blood glucose was measured from a drop of tail vein blood (Accu-Chek Aviva glucometer) at the indicated time points. GTTs in **Fig. 9** were conducted in a 29.5 °C room while all other GTTs were conducted at standard room temperature. For **Fig. 2**, glucose was given by either an intraperitoneal (IP) injection or oral gavage of 2.0 g/kg glucose. For **Figs. 5 & 9**, mice were given IP injections of 1.0 g/kg dextrose (Agri Laboratories, Ltd.) in 0.9% saline (Hospira, Inc.). Insulin concentrations during GTTs (**Figs. 2,9**) were analyzed by RIA by the Vanderbilt University Hormone Assay and Analytical Services Core. In **Fig. 5B**, mice were fasted for 5 h and blood glucose was collected from the tail vein after which the mice were subsequently euthanized by CO_2 and EDTA plasma was collected by cardiac puncture as described, which was stored at -80 °C until insulin was measured by ELISA (Mercodia).

Mouse islet perifusion

Pancreatic islets were isolated and perifusion assays were performed on fresh islets at the Vanderbilt Islet Procurement and Analysis Core as previously described (60). Islet preparations were equilibrated and stable baseline response established at 5.6 mmol/L glucose, and insulin secretion was stimulated

with 16.7 mmol/L glucose. A dose-response curve for the inhibition of GSIS by the α_2AR selective agonist, brimonidine (Br), was generated. Islets were matched for size and number, and assessed as islet equivalents (IEQ) (61).

Energy balance

Food intake and energy expenditure were monitored on mice in a Promethion system (Sable Systems International) by the Vanderbilt Mouse Metabolic Phenotyping Center. The system allows for the continuous high time resolution monitoring of oxygen consumption, carbon dioxide production, feeding and activity patterns and caloric intake. Animals were housed over multiple days to acclimate to the facility. Body weight and composition was monitored before and after a calorimetry study. The calorimetry system is housed in a temperature-controlled cabinet. In some studies animals were housed at standard housing temperature (22 °C) then transitioned to a cold stress (6.0 °C). In other studies, 17-19 weeks old chow-fed mice were transitioned to HFD.

Cardiovascular imaging

Cardiac parameters were measured by parasternal M-mode echocardiography at the VUMC Cardiovascular Physiology Core as described (62, 63). Briefly, mice had their chest fur removed with a topical depilatory agent. Ultrasound coupling gel heated to 34 °C was applied to the chest area and a linear array transducer (18-23 MHz) was positioned to obtain two-dimensional B-mode parasternal long and short axis views at the mid-ventricular level (Vevo 2100, VisualSonics). One-dimensional M-mode images were obtained for measurement in the short axis view to obtain cardiac wall thickness and chamber dimensions. Left ventricular (LV) chamber size and wall thickness were measured off-line in the M-mode from at least three consecutive beats and averaged. LV wall thickness: intraventricular septum (IVS) and posterior wall (PW) at systole and diastole; and LV internal dimensions (LVID) during systole and diastole were measured.

Hyperinsulinemic euglycemic clamps

Clamp studies were done chronically catheterized (carotid artery and jugular vein) conscious mice (64-66). Catheters were inserted 4-5 days prior to a study by the Vanderbilt Mouse Metabolic Phenotyping Center. [3-^{3}H] glucose was used to measure whole body basal and clamp glucose flux. A 4 mU·kg-1·min-1 insulin infusion was initiated to increase insulin to a physiologic range. Red blood cells from a donor animal were infused at a constant rate to replace blood taken during study. Basal and clamp period blood samples for glucose, insulin and tracer. At the end of the clamp period, multiple tissues were collected to measure the accumulation of 2[1-^{14}C]Deoxy-D-glucose(DG). Using tracer methods [3-^{3}H]-glucose and 2[1-^{14}C]DG during the clamp, we assessed tissue glucose uptake and whole body (and hepatic) glucose flux.

Adipo-Clear and three-dimensional imaging

Clearing of inguinal white adipose tissue and staining with sheep polyclonal anti-Tyrosine Hydroxylase (AB1542, Millipore) and rabbit polyclonal anti-UCP1 (ab10983, Abcam) primaries and donkey anti-sheep IgG Alexa Fluor 647 (A-21448, Thermo Fisher Scientific) and donkey anti-rabbit IgG Alexa Fluor 568 (A-10042, Thermo Fisher Scientific) secondaries was performed as described (67). Three-dimensional imaging was performed on a SmartSPIM single-plane illumination light sheet microscope (LifeCanvas Technologies) with a 3.6× objective (NA = 0.2) and axially swept rolling shutter. Samples were illuminated with three excitation wavelengths: 488, 561, and 642 nm. Emissions were detected with 525/50, 600/52, and 680/42 filters. Following acquisition, images were transferred to a Dell Precision 7920 Tower with (2) Intel Xeon Gold 5218R CPU at 2.1 GHz and 256 GB of RAM running Windows 10 Pro for Workstations for stitching and processing.

Images were stitched into Z-stacks with a modified version of Terastitcher and converted to volumetric images using either Imaris for Neuroscience (v 9.8.2, Bitplane, Oxford Instruments, Massachusetts, USA) or syGlass (v7.8.2+) for visualization in virtual reality (ioVision inc, Fountain View, West Virginia, USA). Keyframe animations from the original image data were generated in Imaris. Histogram settings were chosen based on the local region intensity being observed. Using syGlass, the data were

segmented using a maximum intensity projection to distinguish signal from background. Stitched data files (1-2TB per channel) and raw data are stored on a high-performance NAS device (Network Attached Storage; 220TB). All imaging and visualization was performed by the Vanderbilt Neurovisualization Lab, Vanderbilt University.

Western blotting

Adipose tissues were lysed and sonicated in a buffer containing 25 mM HEPES (pH 7.4), 150 mM NaCL, 5 mM EDTA, 5 mM EGTA, 5 mM glycerophosphate, 0.9% Triton X-100, 0.1% IGEPAL, 5 mM sodium pyrophosphate, 10% glycerol, plus 1 tablet each of cOmplete™ protease inhibitor cocktail (04693124001, Roche) and PhoSTOP phosphatase inhibitors (04906845001, Roche) per 10 ml of lysis buffer. The lysates of 40 µg total protein were resolved in 10% Tris-glycine gels, transferred to nitrocellulose membranes, which were incubated overnight at 4 °C with specific primary antibodies, followed by secondary antibody incubations for 1 h at room temperature. The PKA substrate (1:1000, #9624) and β-actin (1:2000, #4967) antibodies were from Cell Signaling Technology (Danvers, MA). Secondary antibodies anti-rabbit (1:20000, A3687) was obtained from MilliporeSigma (Burlington, MA). Image acquisition was performed on Bio-Rad digital ChemiDoc MP with IR (VUMC Molecular Cell Biology Resource).

Catecholamines

For plasma catecholamines, in order to minimize stress-induced catecholamine release mice were cannulated and allowed to move about freely while blood was collected using a blunt needle. Canulations and blood collections were performed by the Vanderbilt Brain Institute Neurochemistry Core. For catecholamines in adipose tissue, whole flash-frozen iWAT was ground into a powder in liquid nitrogen. Powdered iWAT was poured into a tube and weighed. PCA solution (5 mM glutathione in 0.4 N perchloric acid) was added to frozen iWAT powder at a ratio of 1 ml PCA per 100 mg iWAT. Samples were homogenized then centrifuged. The clear supernatant was removed and stored at -80 °C. Catecholamines in both plasma and frozen tissue lysates were analyzed by LC/MS and HPLC

respectively with electrochemical detection as previously described (68) at the Vanderbilt Hormone Assay and Analytical Services Core.

Fecal triglycerides

Feces were collected from the cages of mice that had been fed HFD for 8 weeks and triglycerides were quantified by the VUMC Lipid Core.

Feeding behavior studies

For weekly food intake studies, individually housed animals were given *ad libitum* access to a pre-weighed amount of food which was weighed again at the end of each week. For fasting-refeeding studies, individually housed chow-fed mice were fasted for 12 h before being given *ad libitum* access to preweighed amount of HFD which was weighed hourly. For food-preference studies, individually housed chow-fed mice were given *ad libitum* access to pre-weighed amounts of both chow and HFD. At the end of seven days, chow and HFD were weighed again. Studies were conducted at room temperature unless otherwise stated.

Statistics

Data are mean ± SEM, using GraphPad Prism version 9.1.0(221) for Windows 64-bit (GraphPad Software). Analysis comparing genotype only were performed with an unpaired t-test. Analysis comparing two independent variables were performed with a two-way ANOVA or a mixed-effects model if data were missing. Multiple comparison tests were performed with the Bonferroni correction for SNAP25 genotype only and are indicated on figures by asterisks corresponding to *, $P < .05$; **, $P < .01$; ***, $P < .001$. Whole body energy expenditure data were analyzed using analysis of covariance (48, 49).

Author contributions

Z.Z. conceived the initial idea for the SNAP25$^{\Delta 3/\Delta 3}$ mouse and insulin secretion studies, designed and

led the early research studies, conducted experiments, analyzed data, and contributed to writing the manuscript. R.P.C. designed and led subsequent research studies centered on adipose tissue browning, conducted experiments, analyzed and organized data, wrote manuscript, and made figures. R.P.C. is listed first because he initiated the investigation into the adipocyte browning, led these subsequent studies, and oversaw the final version of the manuscript and figures. A.T.G. managed the mouse colony, conducted experiments, acquired, analyzed, and managed the data. F.A. helped maintain mouse colony and helped conduct mouse studies. F.S. aided in the collection of mouse tissues. D.L. aided in the collection of mouse tissues and performed Western Blots. J.M. performed three-dimensional imaging and made the supplemental movies. J.E.A. designed food intake and metabolic cage studies, analyzed data, and contributed to writing the manuscript. O.P.M. designed experiments, analyzed data, and wrote the manuscript. SC designed experiments and wrote the manuscript. H.H. designed experiments, wrote and organized the manuscript performed and was responsible for the study overall.

Acknowledgements

We would like to thank the following individuals for technical contributions to these studies: Brigitte Jia for helping with mouse tissue collection and helping conduct glucose tolerance tests in a 29.5 °C room. Justice Simonetti for helping maintain the mouse colony and conducting mouse studies, Wei Zhang and Mark Crowder for helping collect mouse tissues, Lin Zhong for conducting echocardiograms experiments and analysis, and Ginger Milne, PhD and Benlian Gao, PhD for the analysis of plasma catecholamine. Al Powers and Greg Poffenberger for conducting islet perifusion studies in the Islet Procurement & Analysis Core of the DRTC. This work was supported by NIH grants DK109204, EY10291, and NS111749 to H.H. R.P.C. was supported by National Institute of Diabetes and Digestive and Kidney Diseases grant F32 DK116520. F.S. was supported by American Diabetes Association grant 1-18-PDF-110. The Vanderbilt Mouse Metabolic Phenotyping Center (MMPC) is supported by

NIH grant DK059637. We acknowledge the Vanderbilt Translational Pathology Shared Resource supported by NCI/NIH Cancer Center Support Grant 5P30 CA68485-19, the Vanderbilt Mouse Metabolic Phenotyping Center Grant 5U24DK059637-13, and the Shared Instrumentation Grant S10 OD023475-01A1 for the Leica Bond RX. Vanderbilt University Hormone Assay and Analytical Services Core and VUMC Lipid Core are supported by NIH grants DK059637 (MMPC) and DK020593 (DRTC). The Islet Procurement & Analysis Core is supported by the Vanderbilt Diabetes Research and Training Center (P60 DK020593). VUMC Cardiovascular Physiology Core is partially supported by NIH U24 DK059637. Vanderbilt University Neurochemistry Core is supported by the Vanderbilt University Brain Institute.

References

1. Tremmel M, Gerdtham UG, Nilsson PM, and Saha S. Economic burden of obesity: A systematic literature review. *Int J Environ Res Public Health.* 2017;14(4).
2. American Diabetes Association. Economic costs of diabetes in the U.S. in 2017. *Diabetes Care.* 2018;41(5):917-28.
3. Hird TR, Zomer E, Owen A, Chen L, Ademi Z, Magliano DJ, et al. The impact of diabetes on productivity in China. *Diabetologia.* 2019;62(7):1195-203.
4. Lopez C, Bendix J, and Sagynbekov K. Weighing down America: 2020 update a community approach against obesity. *Milken Institute.* 2020.
5. Okunogbe A, Nugent R, Spencer G, Ralston J, and Wilding J. Economic impacts of overweight and obesity: current and future estimates for eight countries. *BMJ Glob Health.* 2021;6(10).
6. Ceddia RP, and Collins S. A compendium of G-protein–coupled receptors and cyclic nucleotide regulation of adipose tissue metabolism and energy expenditure. *Clinical Science.* 2020;134(5):473-512.
7. Nauck MA, and Meier JJ. Incretin hormones: Their role in health and disease. *Diabetes Obes Metab.* 2018;20 Suppl 1:5-21.
8. Ahrén B. Islet G protein-coupled receptors as potential targets for treatment of type 2 diabetes. *Nat Rev Drug Discov.* 2009;8(5):369-85.
9. Sriram K, and Insel PA. G protein-coupled receptors as targets for approved drugs: How many targets and how many drugs? *Mol Pharmacol.* 2018;93(4):251-8.
10. Goldsmith ZG, and Dhanasekaran DN. G protein regulation of MAPK networks. *Oncogene.* 2007;26(22):3122-42.
11. Dupré DJ, Robitaille M, Rebois RV, and Hébert TE. The role of Gβγ subunits in the organization, assembly, and function of GPCR signaling complexes. *Annu Rev Pharmacol Toxicol.* 2009;49:31-56.
12. Campbell AP, and Smrcka AV. Targeting G protein-coupled receptor signalling by blocking G proteins. *Nat Rev Drug Discov.* 2018;17(11):789-803.
13. Zhao Y, Fang Q, Straub SG, Lindau M, and Sharp GWG. Noradrenaline inhibits exocytosis via the G protein βγ subunit and refilling of the readily releasable granule pool via the $\alpha_{i1/2}$ subunit. *J Physiol.* 2010;588(Pt 18):3485-98.
14. Zurawski Z, Thompson Gray AD, Brady LJ, Page B, Church E, Harris NA, et al. Disabling the Gβγ-SNARE interaction disrupts GPCR-mediated presynaptic inhibition, leading to physiological and behavioral phenotypes. *Sci Signal.* 2019;12(569).
15. Zurawski Z, Yim YY, Alford S, and Hamm HE. The expanding roles and mechanisms of G protein-mediated presynaptic inhibition. *J Biol Chem.* 2019;294(5):1661-70.
16. Wells CA, Zurawski Z, Betke KM, Yim YY, Hyde K, Rodriguez S, et al. Gβγ inhibits exocytosis via interaction with critical residues on soluble N-ethylmaleimide-sensitive factor attachment protein-25. *Mol Pharmacol.* 2012;82(6):1136-49.
17. Zurawski Z, Rodriguez S, Hyde K, Alford S, and Hamm HE. Gβγ binds to the extreme C terminus of SNAP25 to mediate the action of $G_{i/o}$-coupled G protein-coupled receptors. *Mol Pharmacol.* 2016;89(1):75-83.
18. Irfan M, Zurawski Z, Hamm HE, Bark C, and Stanton PK. Disabling Gβγ-SNAP-25 interaction in gene-targeted mice results in enhancement of long-term potentiation at Schaffer collateral-CA1 synapses in the hippocampus. *Neuroreport.* 2019;30(10):695-9.
19. Bartness TJ, Vaughan CH, and Song CK. Sympathetic and sensory innervation of brown adipose tissue. *Int J Obes (Lond).* 2010;34 Suppl 1:S36-42.
20. Kenny PJ. Reward mechanisms in obesity: New insights and future directions. *Neuron.* 2011;69(4):664-79.
21. Williams KW, and Elmquist JK. From neuroanatomy to behavior: central integration of peripheral

signals regulating feeding behavior. *Nat Neurosci.* 2012;15(10):1350-5.
22. Morrison SF, Madden CJ, and Tupone D. Central neural regulation of brown adipose tissue thermogenesis and energy expenditure. *Cell Metab.* 2014;19(5):741-56.
23. Kim KS, Seeley RJ, and Sandoval DA. Signalling from the periphery to the brain that regulates energy homeostasis. *Nat Rev Neurosci.* 2018;19(4):185-96.
24. Thurmond DC, and Gaisano HY. Recent insights into beta-cell exocytosis in type 2 diabetes. *J Mol Biol.* 2020;432(5):1310-25.
25. Goodpaster BH, and Sparks LM. Metabolic flexibility in health and disease. *Cell Metab.* 2017;25(5):1027-36.
26. Smith RL, Soeters MR, Wüst RCI, and Houtkooper RH. Metabolic flexibility as an adaptation to energy resources and requirements in health and disease. *Endocr Rev.* 2018;39(4):489-517.
27. Thorens B. Neural regulation of pancreatic islet cell mass and function. *Diabetes Obes Metab.* 2014;16 Suppl 1:87-95.
28. Czech MP. Mechanisms of insulin resistance related to white, beige, and brown adipocytes. *Mol Metab.* 2020;34:27-42.
29. Jiang H, Ding X, Cao Y, Wang H, and Zeng W. Dense intra-adipose sympathetic arborizations are essential for cold-induced beiging of mouse white adipose tissue. *Cell Metab.* 2017;26(4):686-92.e3.
30. Guilherme A, Pedersen DJ, Henriques F, Bedard AH, Henchey E, Kelly M, et al. Neuronal modulation of brown adipose activity through perturbation of white adipocyte lipogenesis. *Mol Metab.* 2018;16:116-25.
31. Henriques F, Bedard AH, Guilherme A, Kelly M, Chi J, Zhang P, et al. Single-cell RNA profiling reveals adipocyte to macrophage signaling sufficient to enhance thermogenesis. *Cell Rep.* 2020;32(5):107998.
32. Huesing C, Qualls-Creekmore E, Lee N, François M, Torres H, Zhang R, et al. Sympathetic innervation of inguinal white adipose tissue in the mouse. *J Comp Neurol.* 2021;529(7):1465-85.
33. Huesing C, Zhang R, Gummadi S, Lee N, Qualls-Creekmore E, Yu S, et al. Organization of sympathetic innervation of interscapular brown adipose tissue in the mouse. *J Comp Neurol.* 2021.
34. Münzberg H, Floyd E, and Chang JS. Sympathetic innervation of white adipose tissue: to beige or not to beige? *Physiology (Bethesda).* 2021;36(4):246-55.
35. Cao Y, Wang H, Wang Q, Han X, and Zeng W. Three-dimensional volume fluorescence-imaging of vascular plasticity in adipose tissues. *Mol Metab.* 2018;14:71-81.
36. Wang P, Loh KH, Wu M, Morgan DA, Schneeberger M, Yu X, et al. A leptin–BDNF pathway regulating sympathetic innervation of adipose tissue. *Nature.* 2020;583(7818):839-44.
37. Collins S. A heart-adipose tissue connection in the regulation of energy metabolism. *Nat Rev Endocrinol.* 2014;10(3):157-63.
38. Collins S, Daniel KW, Rohlfs EM, Ramkumar V, Taylor IL, and Gettys TW. Impaired expression and functional activity of the β_3- and β_1-adrenergic receptors in adipose tissue of congenitally obese (C57BL/6J ob/ob) mice. *Mol Endocrinol.* 1994;8(4):518-27.
39. Collins S, Daniel KW, Petro AE, and Surwit RS. Strain-specific response to β_3-adrenergic receptor agonist treatment of diet-induced obesity in mice. *Endocrinology.* 1997;138(1):405-13.
40. Collins S, Daniel KW, and Rohlfs EM. Depressed expression of adipocyte beta-adrenergic receptors is a common feature of congenital and diet-induced obesity in rodents. *Int J Obes Relat Metab Disord.* 1999;23(7):669-77.
41. Kuperman Y, Weiss M, Dine J, Staikin K, Golani O, Ramot A, et al. CRFR1 in AgRP neurons modulates sympathetic nervous system activity to adapt to cold stress and fasting. *Cell Metab.* 2016;23(6):1185-99.
42. Madden CJ, and Morrison SF. Central nervous system circuits that control body temperature. *Neurosci Lett.* 2019;696:225-32.
43. Tan CL, and Knight ZA. Regulation of Body Temperature by the Nervous System. *Neuron.*

2018;98(1):31-48.
44. Riddy DM, Delerive P, Summers RJ, Sexton PM, and Langmead CJ. G protein-coupled receptors targeting insulin resistance, obesity, and type 2 diabetes mellitus. *Pharmacol Rev.* 2018;70(1):39-67.
45. Kalinovich AV, de Jong JM, Cannon B, and Nedergaard J. UCP1 in adipose tissues: two steps to full browning. *Biochimie.* 2017;134:127-37.
46. Kajimura S, Spiegelman BM, and Seale P. Brown and beige fat: Physiological roles beyond heat generation. *Cell Metab.* 2015;22(4):546-59.
47. Tsagkaraki E, Nicoloro SM, DeSouza T, Solivan-Rivera J, Desai A, Lifshitz LM, et al. CRISPR-enhanced human adipocyte browning as cell therapy for metabolic disease. *Nat Commun.* 2021;12(1):6931.
48. Kaiyala KJ, and Schwartz MW. Toward a more complete (and less controversial) understanding of energy expenditure and its role in obesity pathogenesis. *Diabetes.* 2011;60(1):17-23.
49. Corrigan JK, Ramachandran D, He Y, Palmer CJ, Jurczak MJ, Chen R, et al. A big-data approach to understanding metabolic rate and response to obesity in laboratory mice. *Elife.* 2020;9.
50. Jewell JL, Oh E, and Thurmond DC. Exocytosis mechanisms underlying insulin release and glucose uptake: conserved roles for Munc18c and syntaxin 4. *Am J Physiol Regul Integr Comp Physiol.* 2010;298(3):R517-31.
51. Zhu D, Zhang Y, Lam PPL, Dolai S, Liu Y, Cai EP, et al. Dual role of VAMP8 in regulating insulin exocytosis and islet β cell growth. *Cell Metab.* 2012;16(2):238-49.
52. Lam PPL, Ohno M, Dolai S, He Y, Qin T, Liang T, et al. Munc18b is a major mediator of insulin exocytosis in rat pancreatic β-cells. *Diabetes.* 2013;62(7):2416-28.
53. Liang T, Qin T, Kang F, Kang Y, Xie L, Zhu D, et al. SNAP23 depletion enables more SNAP25/calcium channel excitosome formation to increase insulin exocytosis in type 2 diabetes. *JCI Insight.* 2020;5(3).
54. Myers MG, Leibel RL, Seeley RJ, and Schwartz MW. Obesity and leptin resistance: distinguishing cause from effect. *Trends Endocrinol Metab.* 2010;21(11):643-51.
55. Mancini MC, and Halpern A. Investigational therapies in the treatment of obesity. *Expert Opin Investig Drugs.* 2006;15(8):897-915.
56. Hostrup M, and Onslev J. The beta$_2$-adrenergic receptor – a re-emerging target to combat obesity and induce leanness? *J Physiol.* 2022;600(5):1209-27.
57. Mahú I, Barateiro A, Rial-Pensado E, Martinéz-Sánchez N, Vaz SH, Cal PMSD, et al. Brain-Sparing Sympathofacilitators Mitigate Obesity without Adverse Cardiovascular Effects. *Cell Metab.* 2020;31(6):1120-35.e7.
58. Finlin BS, Memetimin H, Zhu B, Confides AL, Vekaria HJ, El Khouli RH, et al. The β3-adrenergic receptor agonist mirabegron improves glucose homeostasis in obese humans. *J Clin Invest.* 2020;130(5):2319-31.
59. O'Mara AE, Johnson JW, Linderman JD, Brychta RJ, McGehee S, Fletcher LA, et al. Chronic mirabegron treatment increases human brown fat, HDL cholesterol, and insulin sensitivity. *J Clin Invest.* 2020;130(5):2209-19.
60. Dai C, Brissova M, Hang Y, Thompson C, Poffenberger G, Shostak A, et al. Islet-enriched gene expression and glucose-induced insulin secretion in human and mouse islets. *Diabetologia.* 2012;55(3):707-18.
61. Brissova M, Shiota M, Nicholson WE, Gannon M, Knobel SM, Piston DW, et al. Reduction in pancreatic transcription factor PDX-1 impairs glucose-stimulated insulin secretion. *J Biol Chem.* 2002;277(13):11225-32.
62. Rottman JN, Ni G, and Brown M. Echocardiographic evaluation of ventricular function in mice. *Echocardiography.* 2007;24(1):83-9.
63. Gao S, Ho D, Vatner DE, and Vatner SF. Echocardiography in Mice. *Curr Protoc Mouse Biol.* 2011;1:71-83.

64. Ayala JE, Bracy DP, McGuinness OP, and Wasserman DH. Considerations in the design of hyperinsulinemic-euglycemic clamps in the conscious mouse. *Diabetes.* 2006;55(2):390-7.
65. Ayala JE, Bracy DP, Malabanan C, James FD, Ansari T, Fueger PT, et al. Hyperinsulinemic-euglycemic clamps in conscious, unrestrained mice. *J Vis Exp.* 2011(57).
66. Hughey CC, Wasserman DH, Lee-Young RS, and Lantier L. Approach to assessing determinants of glucose homeostasis in the conscious mouse. *Mamm Genome.* 2014;25(9-10):522-38.
67. Chi J, Wu Z, Choi CHJ, Nguyen L, Tegegne S, Ackerman SE, et al. Three-Dimensional Adipose Tissue Imaging Reveals Regional Variation in Beige Fat Biogenesis and PRDM16-Dependent Sympathetic Neurite Density. *Cell Metab.* 2018;27(1):226-36.e3.
68. Wong JM, Malec PA, Mabrouk OS, Ro J, Dus M, and Kennedy RT. Benzoyl chloride derivatization with liquid chromatography-mass spectrometry for targeted metabolomics of neurochemicals in biological samples. *J Chromatogr A.* 2016;1446:78-90.

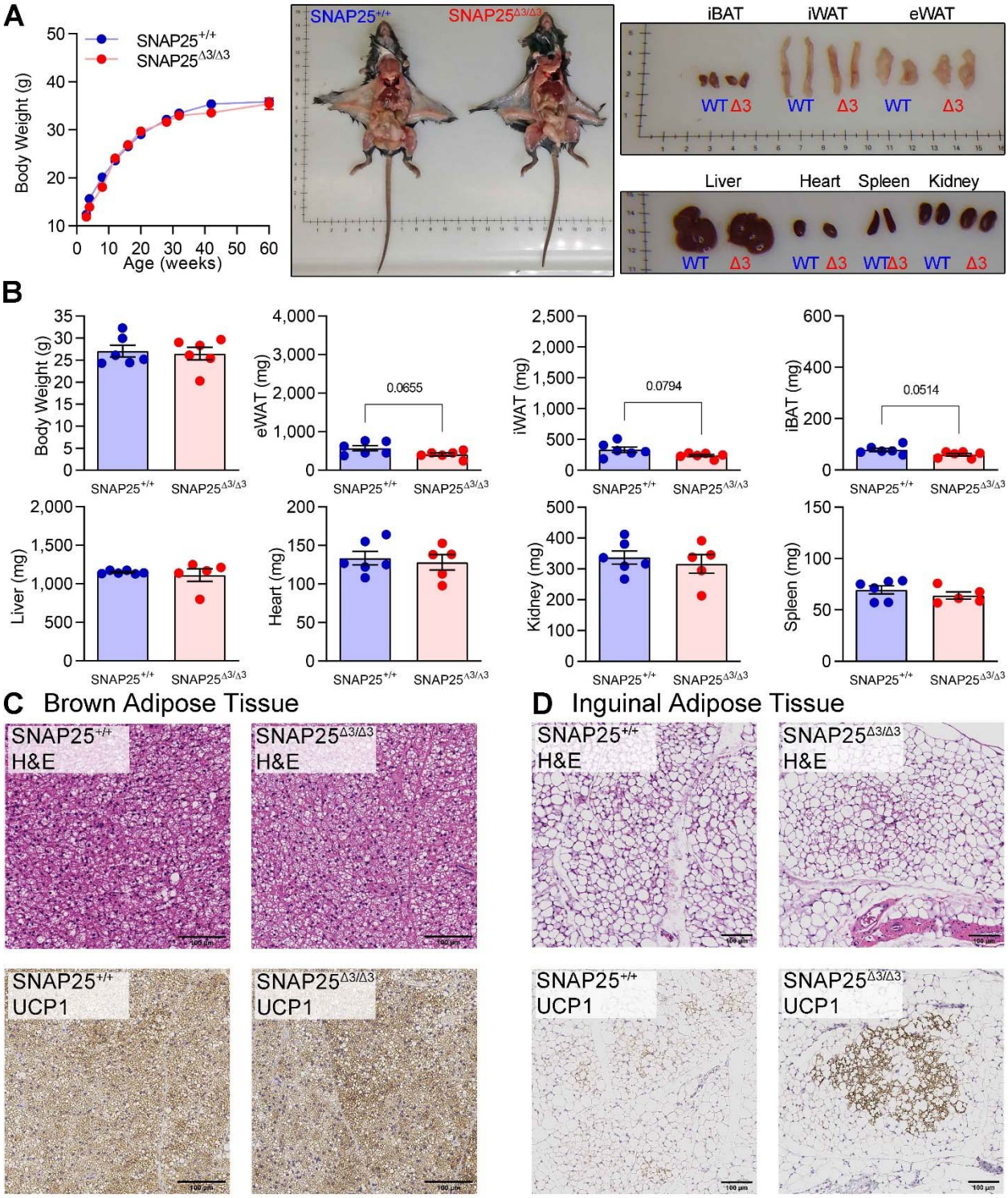
A
SNAP25+/+
SNAP25Δ3/Δ3
Body Weight (g)
Age (weeks)
iBAT
iWAT
eWAT
WT Δ3
Liver
Heart
Spleen
Kidney
B
Body Weight (g)
eWAT (mg)
0.0655
iWAT (mg)
0.0794
iBAT (mg)
0.0514
Liver (mg)
Heart (mg)
Kidney (mg)
Spleen (mg)
C Brown Adipose Tissue
D Inguinal Adipose Tissue
H&E
UCP1

Figure 1. Body and tissue weights are unchanged while white adipose tissue beiging is increased in chow-fed, male SNAP25$^{\Delta3/\Delta3}$ mice

A. Body weights of SNAP25$^{+/+}$ and SNAP25$^{\Delta3/\Delta3}$ male mice were fed standard chow diets (P = 0.3849, effect of genotype; P = 0.0820, effect of genotype × time interaction). *N* = 11 SNAP25$^{+/+}$, 11 SNAP25$^{\Delta3/\Delta3}$. Analysis was performed by two-way ANOVA with repeated measures and post hoc analyses were performed using Bonferroni multiple comparisons test for SNAP25 genotype only. **B.** Body and tissue weights of a separate cohort of chow-fed mice that were euthanized at 15-weeks of age (pictured). *N* = 6 SNAP25$^{+/+}$, 6 SNAP25$^{\Delta3/\Delta3}$. Analyses were performed using t-test. **C.** Representative H&E- and UCP1-stained sections of iBAT. **D.** Representative H&E- and UCP1-stained sections of iWAT. Images are a representative sample from three mice from each group. Values are expressed as mean ± SEM.

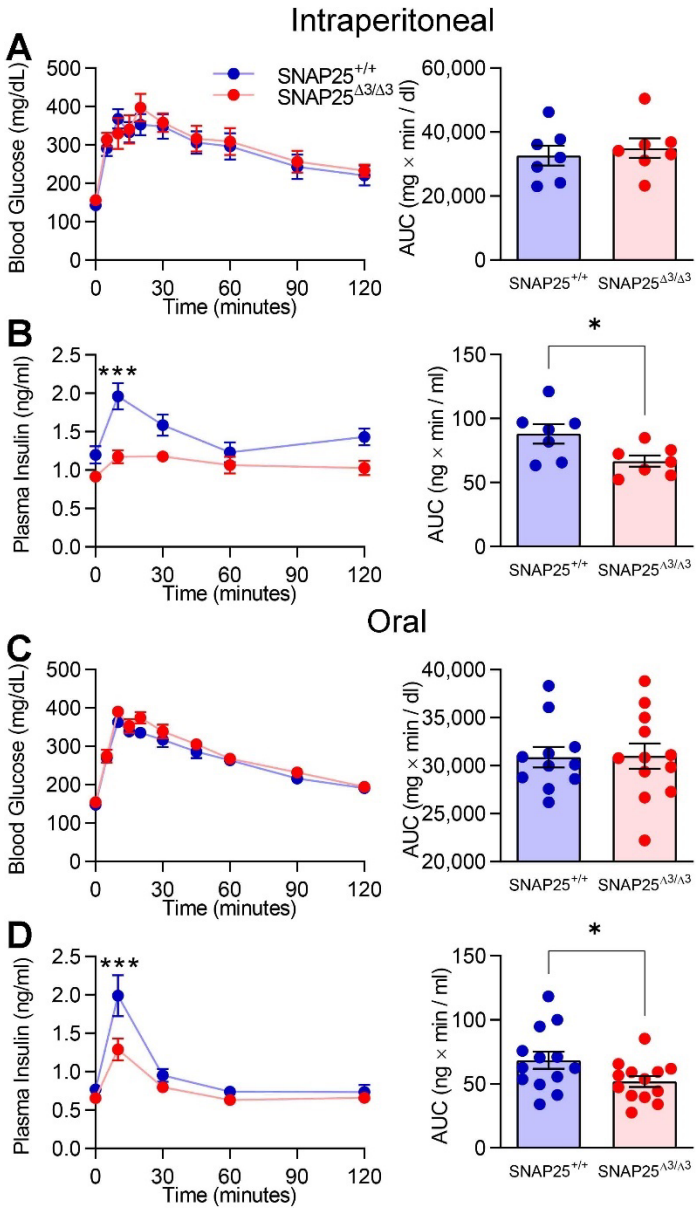
Intraperitoneal
A
Blood Glucose (mg/dL)
Time (minutes)
SNAP25+/+
SNAP25Δ3/Δ3
AUC (mg × min / dl)
B
Plasma Insulin (ng/ml)
***
AUC (ng × min / ml)
*
Oral
C
D

Figure 2. Glucose tolerance is normal but circulating insulin is reduced in chow-fed, male SNAP25$^{\Delta3/\Delta3}$ mice

A. Blood glucose and **B.** plasma insulin levels (P = 0.0176, effect of genotype; P = 0.0031, effect of genotype × time interaction) during an IP-GTT in chow-fed male SNAP25$^{+/+}$ and SNAP25$^{\Delta3/\Delta3}$ at 14 weeks of age. *N* = 8 SNAP25$^{+/+}$, 8 SNAP25$^{\Delta3/\Delta3}$. **C.** Blood glucose and **D.** plasma insulin levels (P = 0.0730, effect of genotype; P = 0.0009, effect of genotype × time interaction) during an oral-GTT in chow-fed male SNAP25$^{+/+}$ and SNAP25$^{\Delta3/\Delta3}$ at 15 weeks of age. *N* = 13 SNAP25$^{+/+}$, 13 SNAP25$^{\Delta3/\Delta3}$. * $p<0.05$. Values are expressed as mean ± SEM. For glucose and insulin time course, two-way ANOVAs were performed with repeated measures and post hoc analyses were performed using Bonferroni multiple comparisons test for SNAP25 genotype only and are indicated on figures. Areas Under the Curve (AUC) were analyzed by t-test.

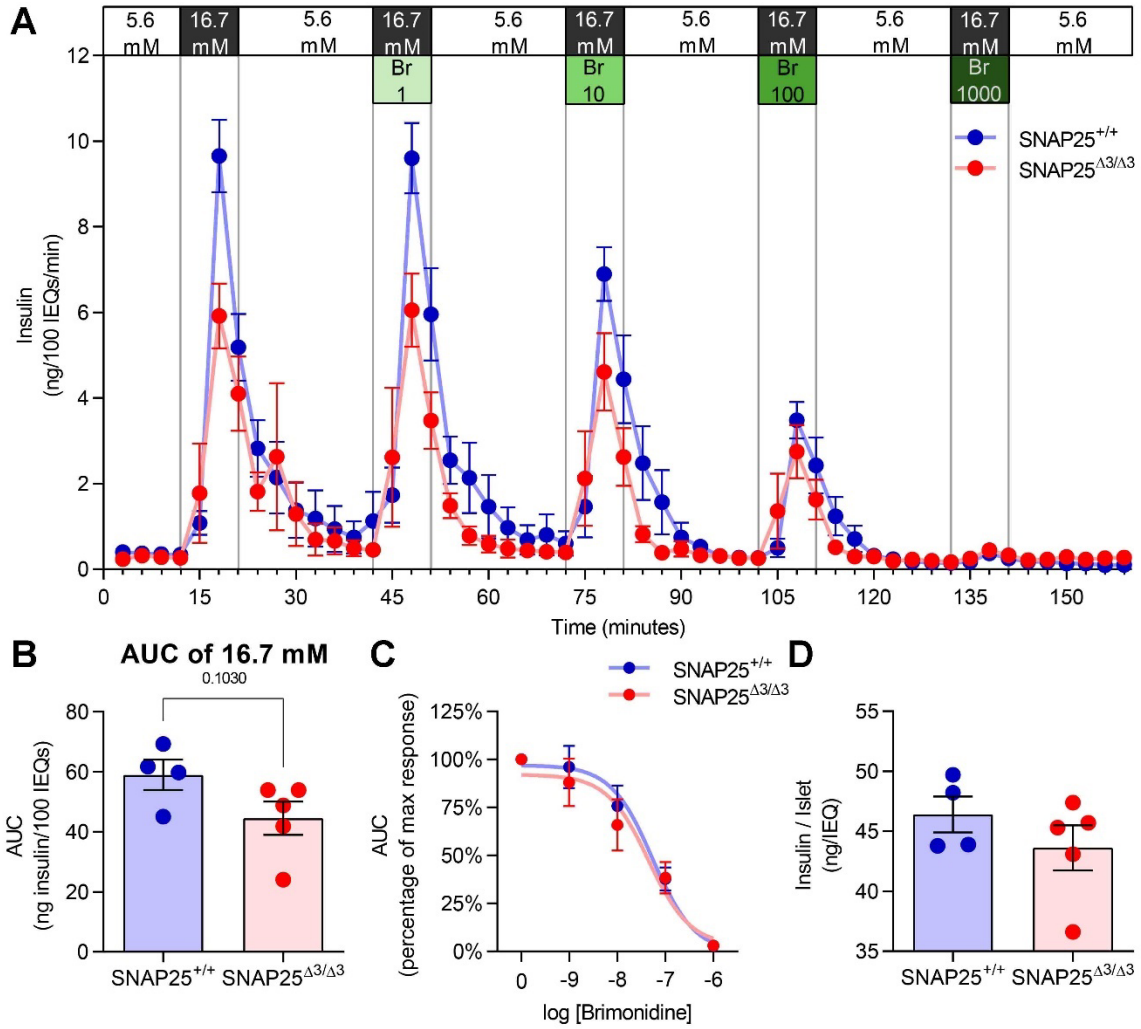
A
5.6 mM
16.7 mM
Br 1
Br 10
Br 100
Br 1000
SNAP25+/+
SNAP25Δ3/Δ3
Insulin (ng/100 IEQs/min)
Time (minutes)
B
AUC of 16.7 mM
0.1030
AUC (ng insulin/100 IEQs)
C
AUC (percentage of max response)
log [Brimonidine]
D
Insulin / Islet (ng/IEQ)

Figure 3. Glucose stimulated insulin secretion is not increased in islets from SNAP25$^{\Delta3/\Delta3}$ mice *ex vivo* and inhibition by α_2AR agonist is not affected by disruption of the Gβγ-SNAP25 interaction

A. Perifusion of islets from 12-week-old male SNAP25$^{+/+}$ and SNAP25$^{\Delta3/\Delta3}$ mice. **B.** Comparison of glucose stimulated insulin secretion (GSIS) between islets from SNAP25$^{+/+}$ and SNAP25$^{\Delta3/\Delta3}$ mice. **C.** AUC values were normalized to the individual's maximal GSIS and a dose-response curve for the inhibition of GSIS by the α_2AR selective agonist, brimonidine (Br), was generated. The log IC50's were similar, being -7.262 for SNAP25$^{+/+}$ and -7.348 for SNAP25$^{\Delta3/\Delta3}$. **D.** Islet insulin content in islets from SNAP25$^{+/+}$ and SNAP25$^{\Delta3/\Delta3}$ mice. For all figures *N* = 4 SNAP25$^{+/+}$, 5 SNAP25$^{\Delta3/\Delta3}$. Values are expressed as mean ± SEM. Analyses were performed using t-test.

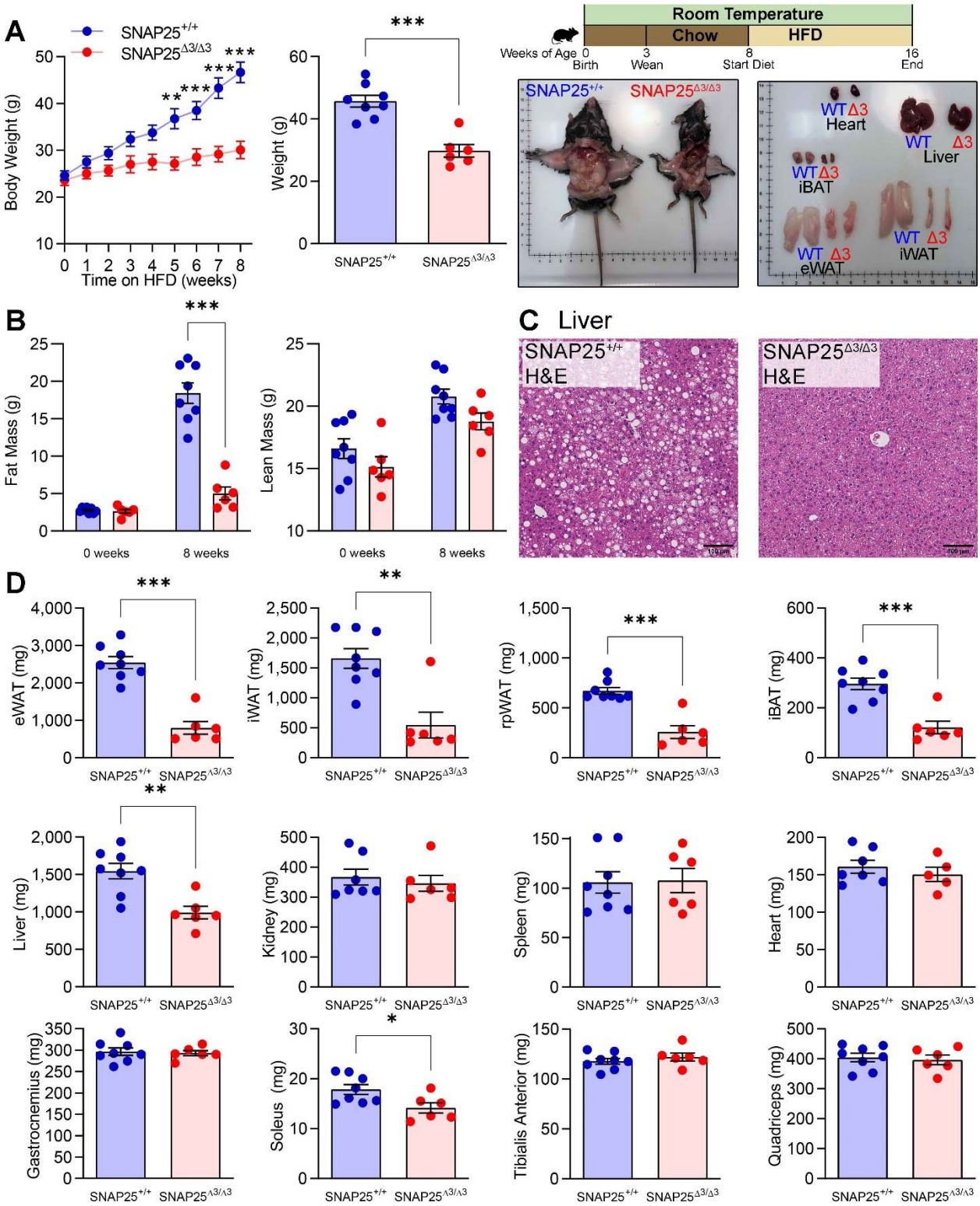
A
SNAP25+/+
SNAP25Δ3/Δ3
Body Weight (g)
Time on HFD (weeks)
Weight (g)
Room Temperature
Chow
HFD
Weeks of Age
Birth
Wean
Start Diet
End
WTΔ3
Heart
Liver
iBAT
eWAT
iWAT
B
Fat Mass (g)
Lean Mass (g)
0 weeks
8 weeks
C Liver
H&E
D
eWAT (mg)
iWAT (mg)
rpWAT (mg)
iBAT (mg)
Liver (mg)
Kidney (mg)
Spleen (mg)
Heart (mg)
Gastrocnemius (mg)
Soleus (mg)
Tibialis Anterior (mg)
Quadriceps (mg)

Figure 4. Weight gain and adiposity induced by HFD are reduced in male SNAP25$^{\Delta3/\Delta3}$ mice

A. Male SNAP25$^{+/+}$ and SNAP25$^{\Delta3/\Delta3}$ were fed HFD for 8 weeks beginning at 8 weeks of age (P = 0.0030, effect of genotype; P < 0.001, effect of genotype × time interaction). Comparison of terminal body weights and representative images of HFD-fed SNAP25$^{+/+}$ and SNAP25$^{\Delta3/\Delta3}$ mice and tissues post-mortem. **B.** Body composition of fat mass (P < 0.001, effect of genotype; P < 0.001, effect of genotype × time interaction) and lean mass (P = 0.0891, effect of genotype) at beginning and end of HFD feeding period. **C.** Representative H&E-stained sections of livers. Images are a representative sample from three mice from each group. **D.** Tissue weights of SNAP25$^{+/+}$ and SNAP25$^{\Delta3/\Delta3}$ mice at the end of the HFD feeding period. For all figures *N* = 8 SNAP25$^{+/+}$, 6 SNAP25$^{\Delta3/\Delta3}$. * p<0.05, ** p<0.01, *** p<0.001. Values are expressed as mean ± SEM. For A (left) and B, two-way ANOVAs were performed with repeated measures and post hoc analyses were performed using Bonferroni multiple comparisons test for SNAP25 genotype only and are indicated on figures. Analyses for terminal body weight (A right) and D were performed using t-test.

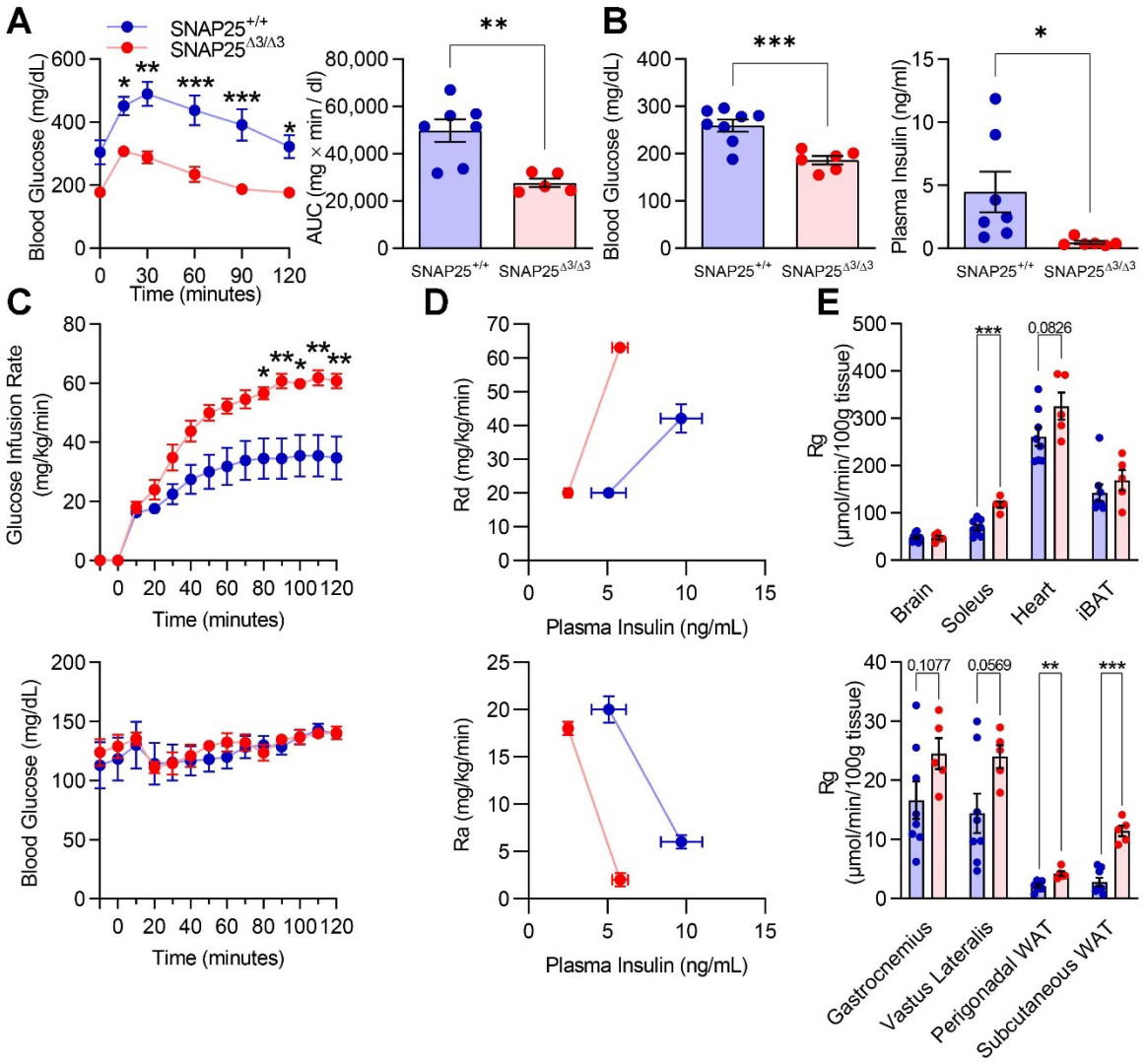
A
SNAP25+/+
SNAP25Δ3/Δ3
Blood Glucose (mg/dL)
Time (minutes)
AUC (mg × min / dl)
B
Blood Glucose (mg/dL)
Plasma Insulin (ng/ml)
C
Glucose Infusion Rate (mg/kg/min)
Time (minutes)
Blood Glucose (mg/dL)
D
Rd (mg/kg/min)
Ra (mg/kg/min)
Plasma Insulin (ng/mL)
E
Rg (μmol/min/100g tissue)
Brain
Soleus
Heart
iBAT
Gastrocnemius
Vastus Lateralis
Perigonadal WAT
Subcutaneous WAT
0.0826
0.1077
0.0569

Figure 5. Insulin action and glucose homeostasis during HFD challenge are improved in male SNAP25$^{\Delta3/\Delta3}$ mice

A. IP-GTT in male SNAP25$^{+/+}$ and SNAP25$^{\Delta3/\Delta3}$ mice fed HFD for 8 weeks (P = 0.0040, effect of genotype; P = 0.0424, effect of genotype × time interaction). *N* = 7 SNAP25$^{+/+}$, 5 SNAP25$^{\Delta3/\Delta3}$. **B.** Fasting blood glucose and plasma insulin levels at euthanasia. *N* = 7-8 SNAP25$^{+/+}$, 6 SNAP25$^{\Delta3/\Delta3}$. **C.** Glucose infusion rate (P = 0.0224, effect of genotype; P < 0.001, effect of genotype × time interaction) and blood glucose levels of HFD-fed SNAP25$^{+/+}$ and SNAP25$^{\Delta3/\Delta3}$ male mice during hyperinsulinemic euglycemic clamp. **D.** Glucose disappearance (Rd) and endogenous glucose production (Ra) plotted against plasma insulin levels. **E.** Tissue [^{14}C]2-deoxy-D-glucose uptake (Rg). For C-E, *N* = 8 SNAP25$^{+/+}$, 5 SNAP25$^{\Delta3/\Delta3}$. ** p<0.01, *** p<0.001. Values are expressed as mean ± SEM. For A D, and C (glucose and GIR), two-way ANOVA was performed with repeated measures and post hoc analyses were performed using Bonferroni multiple comparisons test for SNAP25 genotype only and are indicated on figures. For A (AUC) B and E, analyses were analyzed by t-test

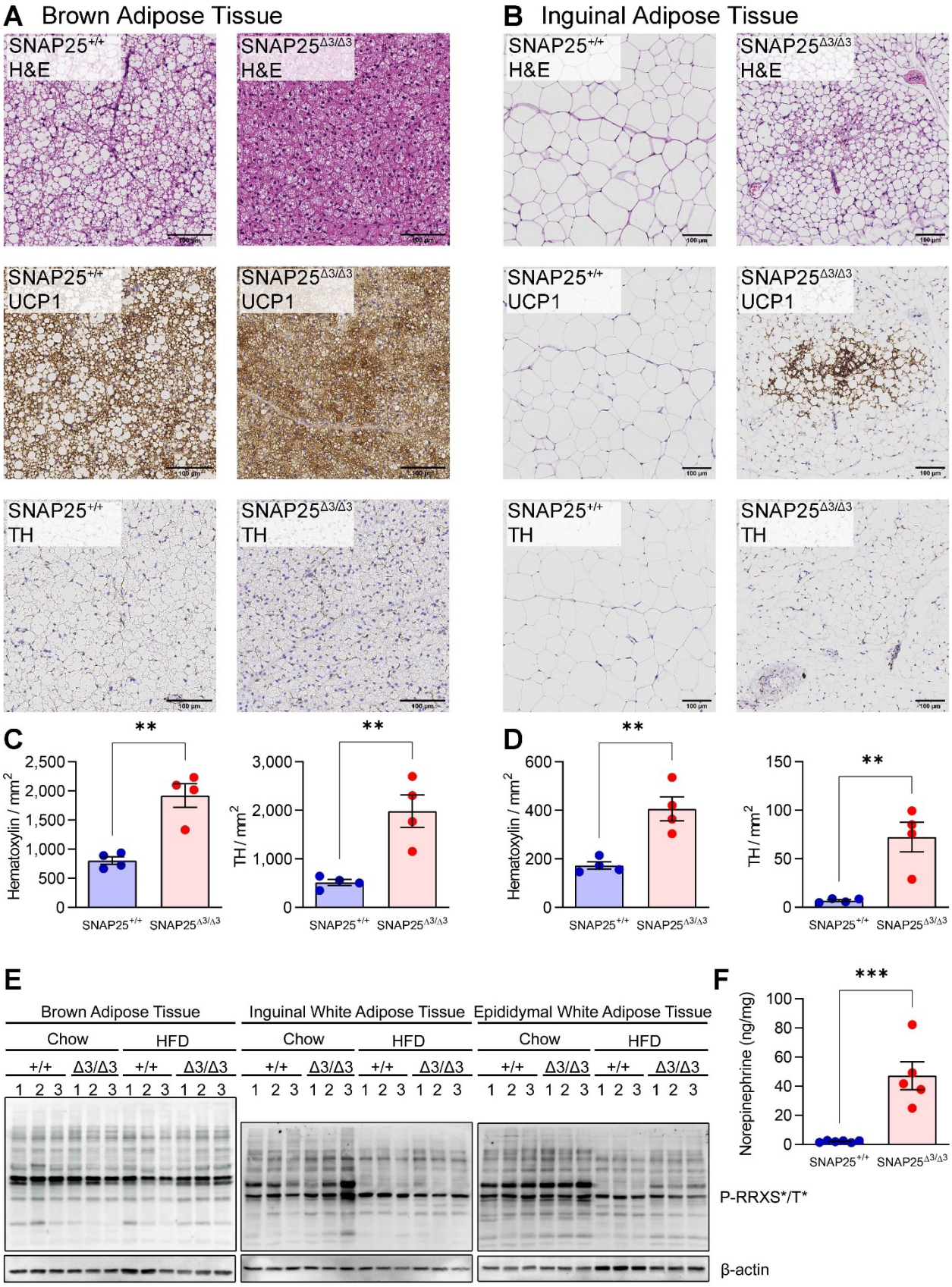
A Brown Adipose Tissue
B Inguinal Adipose Tissue
SNAP25+/+ H&E
SNAP25Δ3/Δ3 H&E
SNAP25+/+ UCP1
SNAP25Δ3/Δ3 UCP1
SNAP25+/+ TH
SNAP25Δ3/Δ3 TH
C
D
Hematoxylin / mm2
TH / mm2
SNAP25+/+
SNAP25Δ3/Δ3
E
Brown Adipose Tissue
Inguinal White Adipose Tissue
Epididymal White Adipose Tissue
Chow
HFD
+/+
Δ3/Δ3
P-RRXS*/T*
β-actin
F
Norepinephrine (ng/mg)

Figure 6. Adipose tissue remodeling in response to HFD is replaced by increased norepinephrine-PKA signaling and beiging in SNAP25$^{\Delta3/\Delta3}$ mice

A. Representative H&E-, UCP1-, and TH-stained sections of iBAT. **B.** Representative H&E-, UCP1-, and TH-stained sections of iWAT. **C.** Quantification of nuclei (hematoxylin) and TH-positive neurons in the iBAT TH-stained slides. **D.** Quantification of nuclei (hematoxylin) and TH-positive neurons in the iWAT TH-stained slides. Images are a representative sample from three to four mice from each group. **E.** Phospho-PKA substrate Western Blot from iBAT, iWAT, and eWAT of chow- and HFD-fed SNAP25$^{+/+}$ and SNAP25$^{\Delta3/\Delta3}$ male mice. **F.** Norepinephrine content of iWAT from HFD-fed SNAP25$^{+/+}$ and SNAP25$^{\Delta3/\Delta3}$ male mice. N = 6 SNAP25$^{+/+}$, 5 SNAP25$^{\Delta3/\Delta3}$. ** $p<0.01$, *** $p<0.001$. Values are expressed as mean ± SEM. Analyses were performed using t-test.

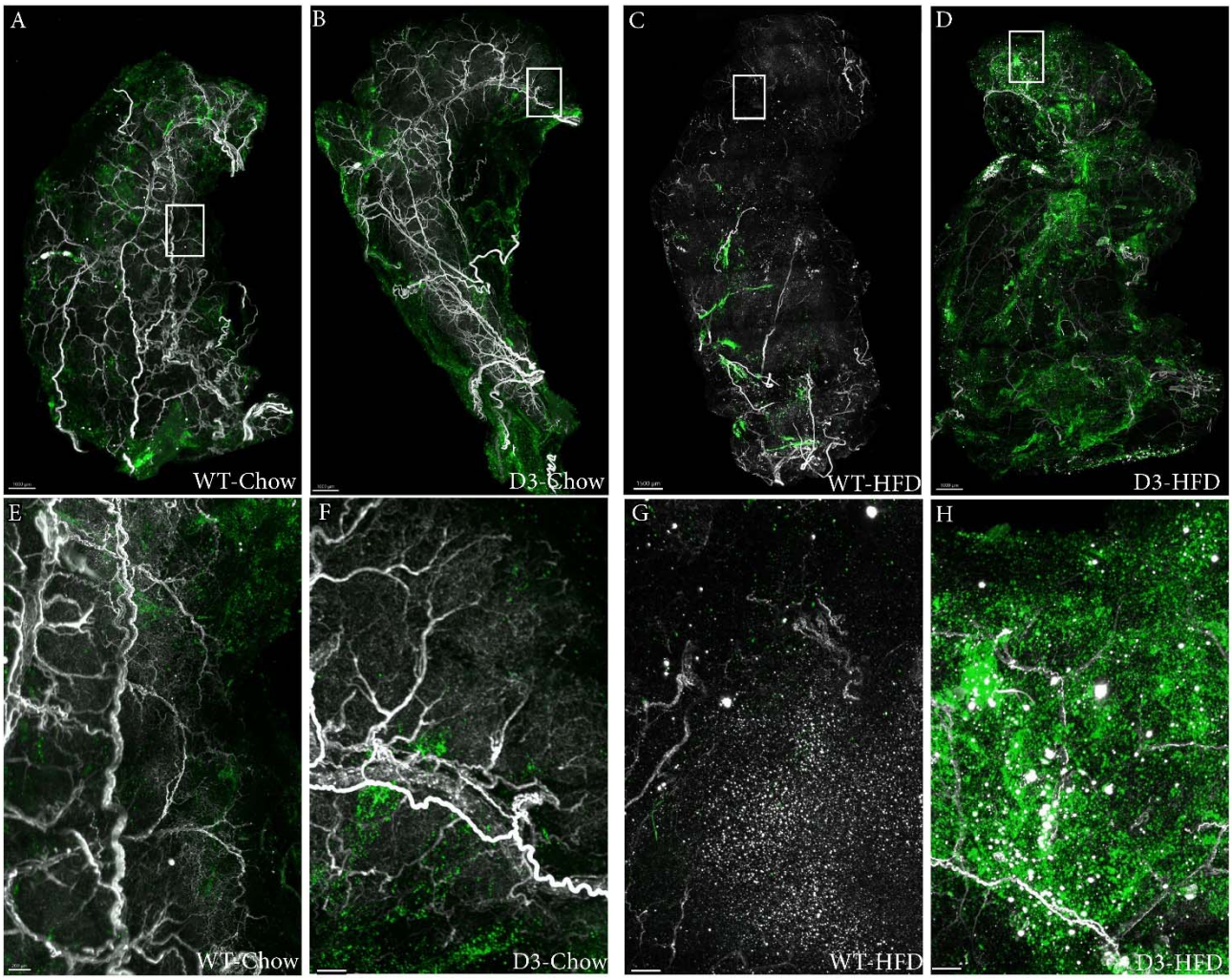
A
WT-Chow
B
D3-Chow
C
WT-HFD
D
D3-HFD
E
WT-Chow
F
D3-Chow
G
WT-HFD
H
D3-HFD

Figure 7. Representative three-dimensional images of cleared inguinal white adipose tissue

Representative 3-D images of cleared iWAT co-stained for TH (white) and UCP1 (green). **A.** Chow-fed SNAP25$^{+/+}$. **B.** Chow-fed SNAP25 $^{\Delta 3/\Delta 3}$. **C.** HFD-fed SNAP25$^{+/+}$. **D.** HFD-fed SNAP25 $^{\Delta 3/\Delta 3}$. **E.** Higher magnification of chow-fed SNAP25$^{+/+}$. **F.** Higher magnification of chow-fed SNAP25 $^{\Delta 3/\Delta 3}$. **G.** Higher magnification of HFD-fed SNAP25$^{+/+}$. **H.** Higher magnification of HFD-fed SNAP25 $^{\Delta 3/\Delta 3}$. Images are a representative sample from three to four mice from each group.

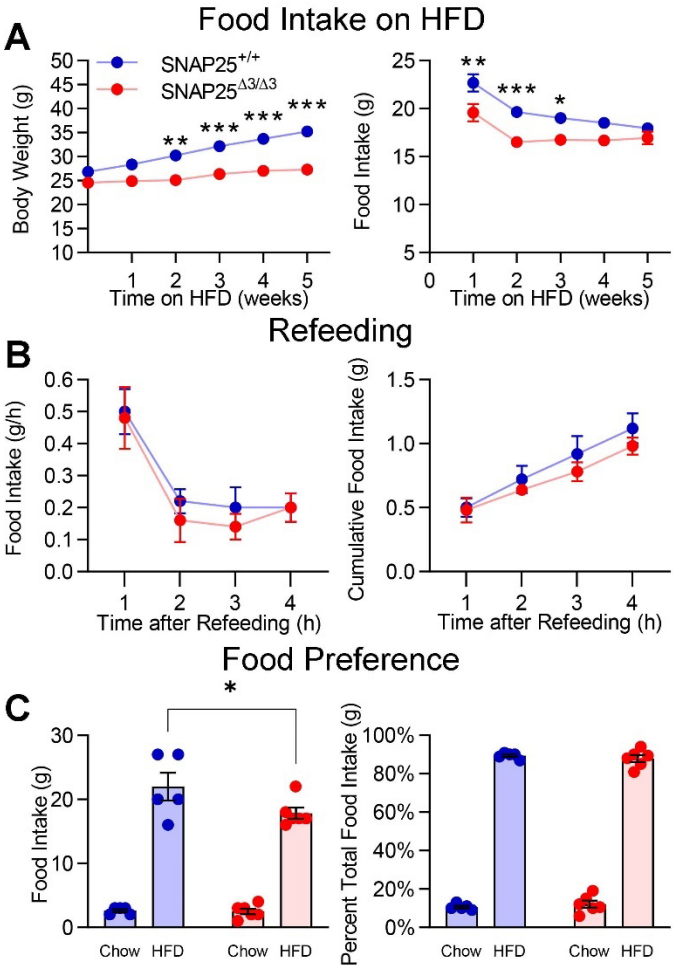
A
Food Intake on HFD
SNAP25+/+
SNAP25Δ3/Δ3
Body Weight (g)
Time on HFD (weeks)
Food Intake (g)
Time on HFD (weeks)
B
Refeeding
Food Intake (g/h)
Time after Refeeding (h)
Cumulative Food Intake (g)
Time after Refeeding (h)
C
Food Preference
Food Intake (g)
Chow HFD Chow HFD
Percent Total Food Intake (g)
Chow HFD Chow HFD

Figure 8. Initial hyperphagic response to HFD is attenuated without differences in fasting-induced hyperphagia or dietary preference in male SNAP25$^{\Delta3/\Delta3}$ mice

A. Body weight ($P < 0.001$, effect of genotype; $P < 0.001$, effect of genotype × time interaction) and food consumption ($P < 0.001$, effect of genotype; $P = 0.2466$, effect of genotype × time interaction) during the first 5-weeks of HFD feeding in a separate cohort of male SNAP25$^{+/+}$ and SNAP25$^{\Delta3/\Delta3}$ mice. *N* = 23 SNAP25$^{+/+}$, 18 SNAP25$^{\Delta3/\Delta3}$. **B.** Consumption of HFD in male SNAP25$^{+/+}$ and SNAP25$^{\Delta3/\Delta3}$ mice following a 12-hour fast. *N* = 5 SNAP25$^{+/+}$, 5 SNAP25$^{\Delta3/\Delta3}$. **C.** Cumulative food intake from chow adapted male SNAP25$^{+/+}$ and SNAP25$^{\Delta3/\Delta3}$ mice given *ad libitum* access to both chow and HFD. *N* = 5 SNAP25$^{+/+}$, 6 SNAP25$^{\Delta3/\Delta3}$. * $p<0.05$, ** $p<0.01$, *** $p<0.001$. Values are expressed as mean ± SEM. Analyses were performed using two-way ANOVA and post hoc analyses were performed using Bonferroni multiple comparisons test for SNAP25 genotype only and are indicated on figures.

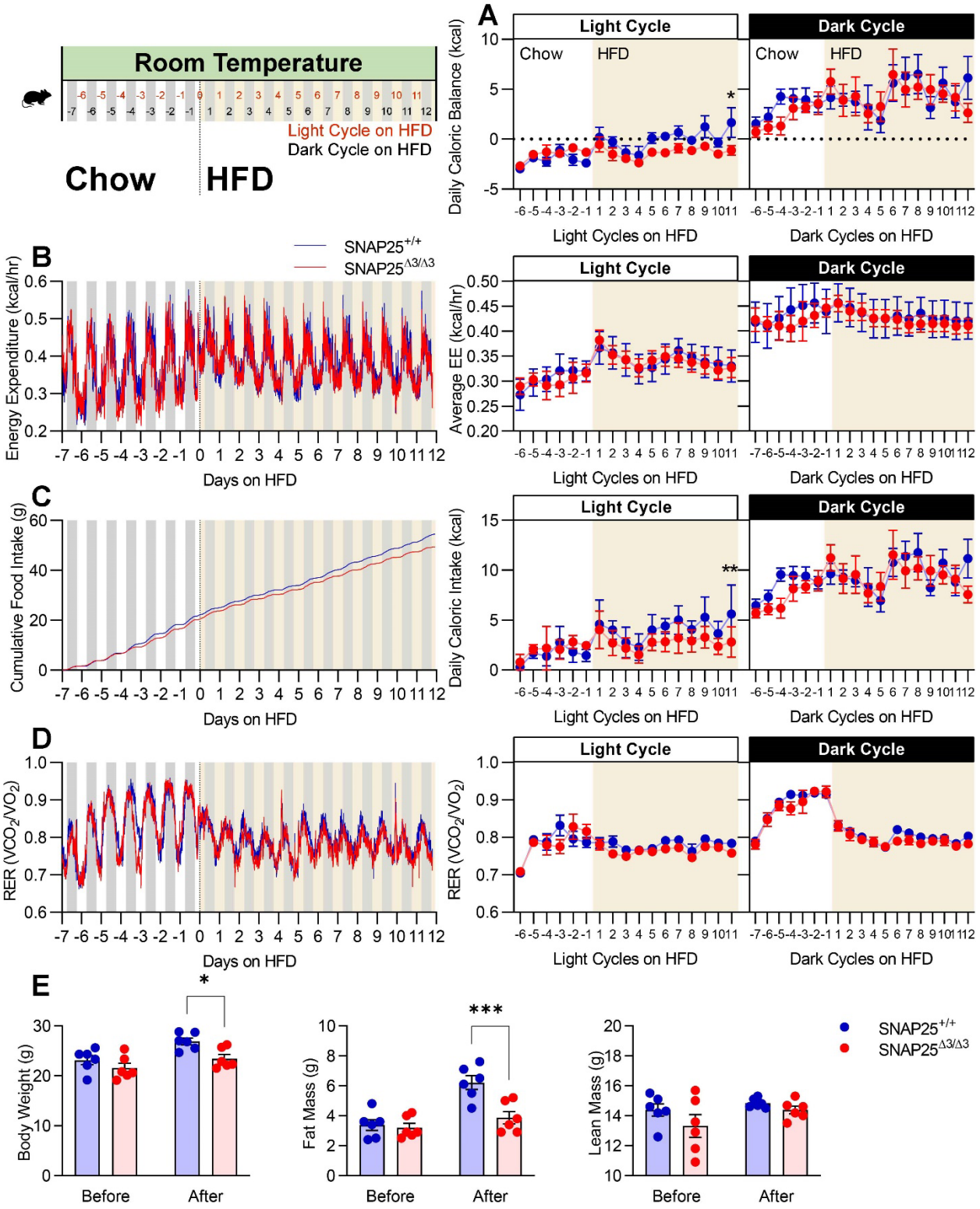
Room Temperature
Light Cycle on HFD
Dark Cycle on HFD
Chow
HFD
A
Light Cycle
Dark Cycle
Daily Caloric Balance (kcal)
Light Cycles on HFD
Dark Cycles on HFD
B
SNAP25+/+
SNAP25Δ3/Δ3
Energy Expenditure (kcal/hr)
Days on HFD
Average EE (kcal/hr)
C
Cumulative Food Intake (g)
Daily Caloric Intake (kcal)
D
RER (VCO2/VO2)
E
Body Weight (g)
Fat Mass (g)
Lean Mass (g)
Before
After

Figure 9. Lower net caloric accumulation upon transition to HFD is associated with lesser food intake without alterations in energy expenditure in male SNAP25$^{\Delta 3/\Delta 3}$ mice

Chow-fed twelve-week-old male SNAP25$^{+/+}$ and SNAP25$^{\Delta 3/\Delta 3}$ mice were acclimated in the Promethion System for one week prior to transitioning to HFD. **A.** Energy balance (P = 0.0006 for the effect of genotype × time during the light cycle). **B.** Energy expenditure. **C.** Cumulative food intake (P = 0.0556 for the effect of genotype; P = 0.0023 for the effect of genotype × time during the light cycle). **D.** Respiratory exchange ratio. **E.** Body weights and composition before (day -7) and after (day 12) these energy balance studies. For all figures, *N* = 6 SNAP25$^{+/+}$, 6 SNAP25$^{\Delta 3/\Delta 3}$. * p<0.05, *** p<0.001. Light and dark cycles were analyzed separately. Analyses were performed by two-way ANOVA with repeated measures and post hoc analyses were performed using Bonferroni multiple comparisons test for SNAP25 genotype only. Energy expenditure was assessed using ANCOVA.

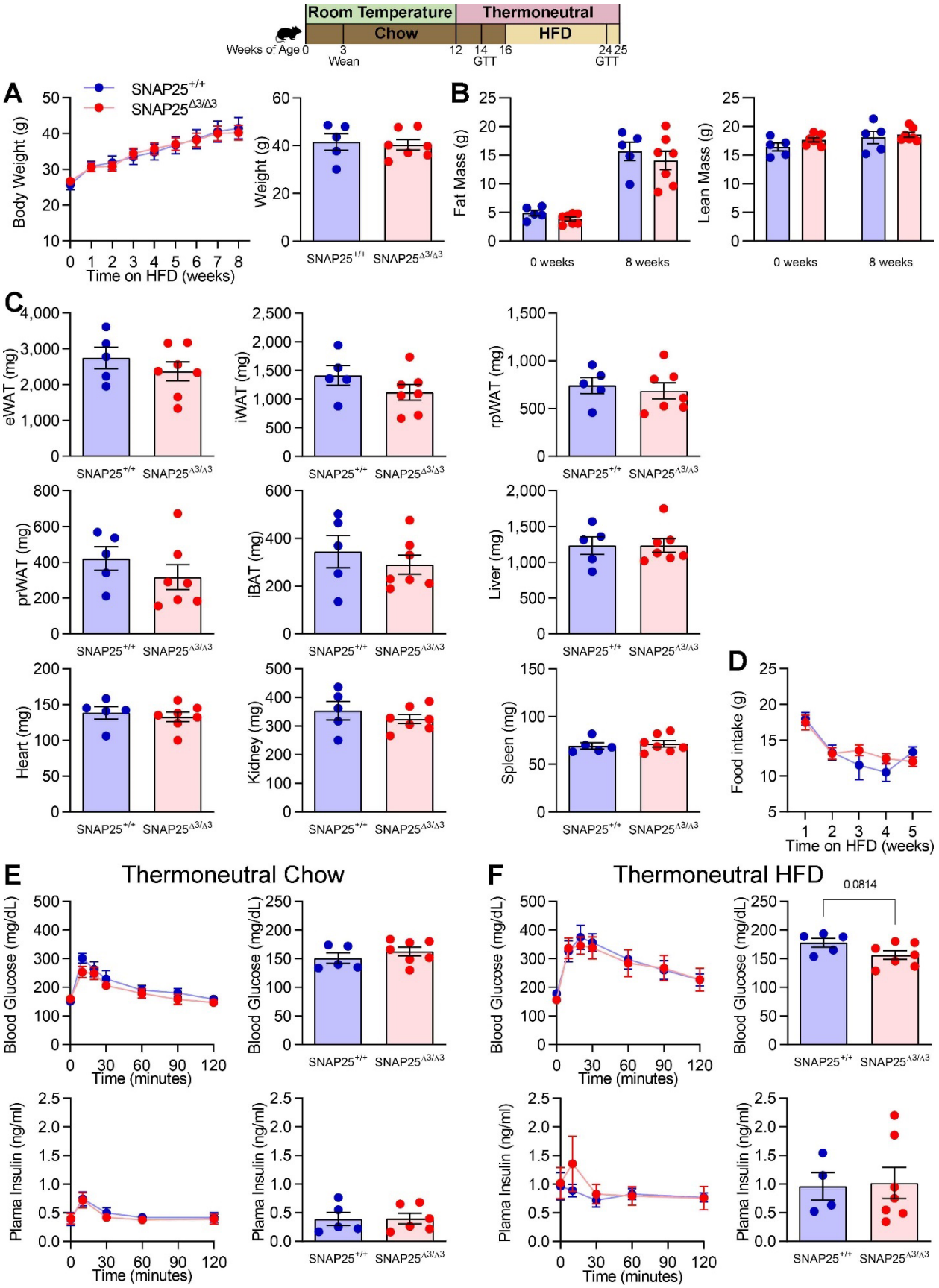
Room Temperature
Thermoneutral
Chow
HFD
Weeks of Age 0 3 12 14 16 24 25
Wean
GTT
GTT
A
SNAP25+/+
SNAP25Δ3/Δ3
Body Weight (g)
Time on HFD (weeks)
Weight (g)
B
Fat Mass (g)
Lean Mass (g)
0 weeks
8 weeks
C
eWAT (mg)
iWAT (mg)
rpWAT (mg)
prWAT (mg)
iBAT (mg)
Liver (mg)
Heart (mg)
Kidney (mg)
Spleen (mg)
D
Food intake (g)
Time on HFD (weeks)
E
Thermoneutral Chow
Blood Glucose (mg/dL)
Time (minutes)
Plama Insulin (ng/ml)
F
Thermoneutral HFD
0.0814

Figure 10. Lack of metabolic protection during HFD feeding in male SNAP25$^{\Delta3/\Delta3}$ mice under thermoneutral housing conditions

A. Following 4 weeks of acclimation to thermoneutral housing conditions, male SNAP25$^{+/+}$ and SNAP25$^{\Delta3/\Delta3}$ were fed HFD for 8 weeks. Comparison of terminal body weights. **B.** Body composition at beginning and end of HFD feeding period. **C.** Tissue weights of SNAP25$^{+/+}$ and SNAP25$^{\Delta3/\Delta3}$ mice at the end of the HFD feeding period. **D.** Food consumption during the first 5-weeks of HFD feeding during thermoneutral housing conditions. *N* = 5 SNAP25$^{+/+}$, 7 SNAP25$^{\Delta3/\Delta3}$. Analysis was performed by two-way ANOVA with repeated measures and post hoc analyses were performed using Bonferroni multiple comparisons test for SNAP25 genotype only. **E.** Blood glucose and plasma insulin levels during an IP-GTT in chow-fed male SNAP25$^{+/+}$ and SNAP25$^{\Delta3/\Delta3}$ housed at thermoneutral conditions for two weeks. Fasting blood glucose and plasma insulin at “time 0” of GTT. **F.** Blood glucose and plasma insulin levels during an IP-GTT in HFD-fed male SNAP25$^{+/+}$ and SNAP25$^{\Delta3/\Delta3}$ housed at thermoneutral conditions. Fasting blood glucose and plasma insulin at “time 0” of GTT. For all figures *N* = 5 SNAP25$^{+/+}$, 6-7 SNAP25$^{\Delta3/\Delta3}$. Values are expressed as mean ± SEM. Most analyses were performed by two-way ANOVAs with repeated measures and post hoc analyses were performed using Bonferroni multiple comparisons test for SNAP25 genotype only. Exceptions were terminal body weight (A right), tissue weights (C), and fasting glucose and insulin (D and E right), which were performed using t-test.

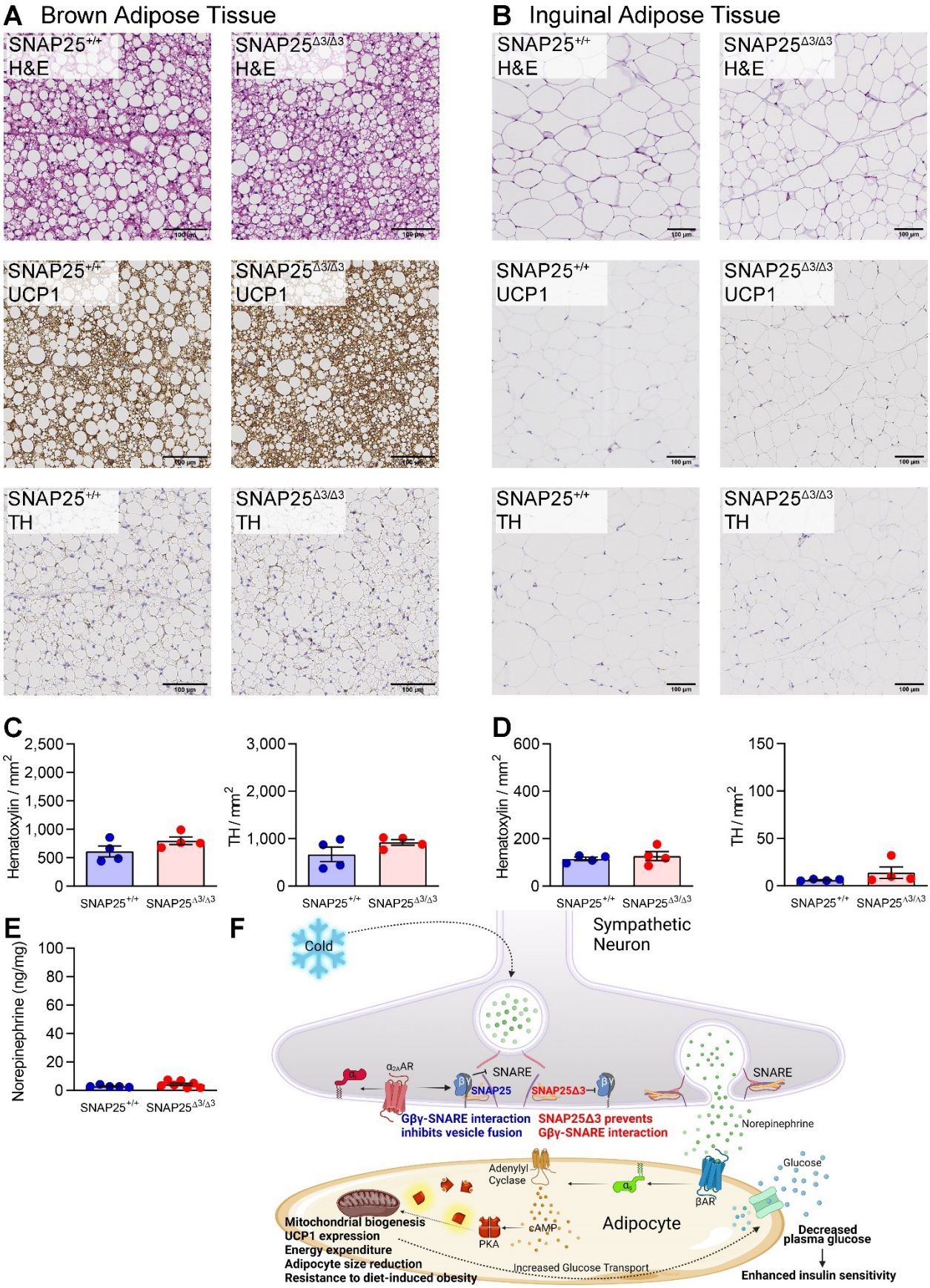
A Brown Adipose Tissue
B Inguinal Adipose Tissue
SNAP25+/+ H&E
SNAP25Δ3/Δ3 H&E
SNAP25+/+ UCP1
SNAP25Δ3/Δ3 UCP1
SNAP25+/+ TH
SNAP25Δ3/Δ3 TH
C
Hematoxylin / mm2
TH / mm2
D
E
Norepinephrine (ng/mg)
F
Cold
Sympathetic Neuron
α2AAR
SNARE
SNAP25
SNAP25Δ3
Gβγ-SNARE interaction inhibits vesicle fusion
SNAP25Δ3 prevents Gβγ-SNARE interaction
Norepinephrine
Glucose
Adenylyl Cyclase
βAR
cAMP
PKA
Adipocyte
Mitochondrial biogenesis
UCP1 expression
Energy expenditure
Adipocyte size reduction
Resistance to diet-induced obesity
Increased Glucose Transport
Decreased plasma glucose
Enhanced insulin sensitivity

Figure 11. Adipose tissue expansion in response to HFD without beiging in SNAP25$^{\Delta3/\Delta3}$ male mice during thermoneutral housing conditions

A. Representative H&E-, UCP1-, and TH-stained sections of iBAT. **B.** Representative H&E-, UCP1-, and TH-stained sections of iWAT. **C.** Quantification of nuclei (hematoxylin) and TH-positive neurons in the iBAT TH-stained slides. **D.** Quantification of nuclei (hematoxylin) and TH-positive neurons in the iWAT TH-stained slides. Images are a representative sample from three to four mice from each group. **E.** Norepinephrine content of iWAT from HFD-fed SNAP25$^{+/+}$ and SNAP25$^{\Delta3/\Delta3}$ male mice. *N* = 5 SNAP25$^{+/+}$, 7 SNAP25$^{\Delta3/\Delta3}$. Values are expressed as mean ± SEM. All analyses were performed using t-test. **F**. Summary Figure: During cold stress, sympathetic regulation of adipocyte beiging/browning occurs through release of NE from sympathetic neurons and thereby induction of the adipocyte β-adrenergic program. This increases mitochondrial biogenesis (browning) and expression of UCP1 generating heat by expending energy through uncoupled respiration. Housing mice at room temperature (normal housing around 22 °C) evokes a mild cold stress that is generally unnoticed. Normally there is an α_{2A}-adrenergic brake on neurotransmitter vesicle fusion that works through the Gβγ-SNARE interaction limiting NE release. We have removed this brake on NE release by creating a mutant SNAP25 that decreases Gβγ binding leading to increased NE release, greater β-adrenergic signaling, and induction of the adipocyte thermogenic program. This causes beiging of white adipose tissue and the increased fuel utilization reduces lipid droplet size in both white and brown depots leading to smaller adipocytes. This enhanced browning increases glucose uptake into beige adipocytes leading to enhanced insulin sensitivity, particularly in these white adipose depots. A result of these adaptations in SNAP25$^{\Delta3/\Delta3}$ animals is resistance to diet-induced obesity. In addition, adipocyte browning feeds back onto sympathetic neurons, increasing the number of adrenergic boutons containing TH. Removal of the cold-induced sympathetic tone by placing animals under thermoneutral conditions (~30 °C) reverses all of these changes, allowing us to conclude that the inability of Gβγ to act as a negative regulator of NE release is the main driver of the beneficial metabolic phenotype.